Electrochemistry Communications 95 (2018) 5–8

Contents lists available at ScienceDirect

Electrochemistry Communications

journal homepage: www.elsevier.com/locate/elecom

Covalent grafting of fluoride-encapsulating silsesquioxane $F^-@Ph_8T_8$ onto glassy carbon

Amel Farhati[a], Mikhail Syroeshkin[b], Mohammed Dammak[a], Viatcheslav Jouikov[c,*]

[a] University of Sfax, Faculty of Sciences, 3000 BP, 1171 Sfax, Tunisia
[b] N.D. Zelinsky Institute of Organic Chemistry RAS, 119991 Moscow, Russia
[c] UMR 6226 ISCR, University of Rennes I, 35042 Rennes, France

ARTICLE INFO

Keywords:
Glassy carbon
Functionalization
Fluoride encapsulating
Silsesquioxane
Sensing

ABSTRACT

Covalent immobilization of fluoride-encapsulating octaphenyl silsesquioxane $F^-@Ph_8T_8$ on glassy carbon (GC) was achieved using a new ambifunctional grafting agent, iodomethyltrimethylsilane $TMSCH_2I$. This grafting method did not require any pre-grafting functionalization of the Ph-trimmed substrate; instead, the GC interface was anodically covered with CH_2I groups whose ensuing reduction in the presence of $F^-@Ph_8T_8$ resulted in the covalent grafting of the phenyl silsesquioxane cage onto the GC surface via the CH_2 linker(s). The resulting ionic interface can be used to detect exposure to Li^+- and H^+-containing media. The proposed electrochemical process offers a general method for covalent binding of two (poly)aromatic substrates by a methylene bridge.

1. Introduction

Making an electrochemical sensor usually involves immobilization of an appropriate system with a redox response specific to an external event, on a conductive support [1]. Recently discovered octa-organo silsesquioxanes encapsulating a F^- anion $F^-@R_8T_8$ [2,3] have (at least) two particular properties that might be interesting for making sensing devices – their non-coordinating and non-nucleophilic anionic nature [4,5], and their ability to release a F^- anion from their otherwise stable cage structure in the presence of Li^+ and H^+ cations [6].

Octaphenyl silsesquioxane Ph_8T_8 has cubic symmetry with six equivalent faces, resembling a dice (Scheme 1), with eight Ph groups at the vertices by which this system can be attached to the surface. When deposited on a conductive support, the Ph_8T_8 cage therefore has up to four possibilities for the covalent immobilization – one for each Ph group. It might seem straightforward to achieve this grafting via reduction of aryldiazonium salts. However, this well-developed method [7–9] requires the preparation of diazoderivatives of the substrate to be immobilized [9–11]. Apart from the fact that amination of the parent Ph_8T_8 is quite complex [12], the direct aryldiazonium method of immobilizing $F^-@R_8T_8$ is impossible for electronic reasons [13,14], because F-encapsulating silsesquioxanes can only be prepared with non-donor R groups (i.e. $R \neq C_6H_4NH_2$ [4,6]). Therefore, in order to covalently immobilize the $F^-@R_8T_8$ unit as is, without transforming it to a diazoderivative or requiring any other chemical modification of its Ph groups, we used the ambifunctional grafting reagent $TMSCH_2I$. This allows a "pre-glued" surface to be prepared, taking advantage of the recently introduced method of anodic grafting with TMS-containing precursors or linkers [15,16], followed by cathodic grafting based on the reduction of CH_2I. We report here on the covalent immobilization of this particular system at a glassy carbon surface, allowing one to obtain a non-leaking and non-washable F^--loaded ionic interface sensitive to the presence of Li^+ and H^+ cations.

2. Experimental

Electrochemical measurements and grafting were performed using a PAR-2273 potentiostat controlled by the PowerSuite package [17] in a three-electrode mode using a standard 25 mL electrochemical cell. SEM-EDS mapping analysis was performed with a JEOL JSM 7100 F spectrometer with an EDS SDD X-Max 50 mm^2 Oxford Instruments AZtecEnergy detector at CMEBA (University Rennes 1).

CH_3CN (Acros) was distilled over CaH_2 under argon and the supporting electrolyte $TBAPF_6$ (Fluka) was dried overnight under a vacuum at 80 °C before use. F-encapsulating silsesquioxane salt $F^-@Ph_8T_8[TBA^+]$ was prepared from $PhSi(OEt)_3$ (ABCR) and TBAF (Acros) as described previously [3]. $TMSCH_2I$ was purchased from ABCR and used as received.

* Corresponding author.
E-mail address: vjouikov@univ-rennes1.fr (V. Jouikov).

https://doi.org/10.1016/j.elecom.2018.08.011
Received 1 August 2018; Received in revised form 20 August 2018; Accepted 21 August 2018
Available online 23 August 2018

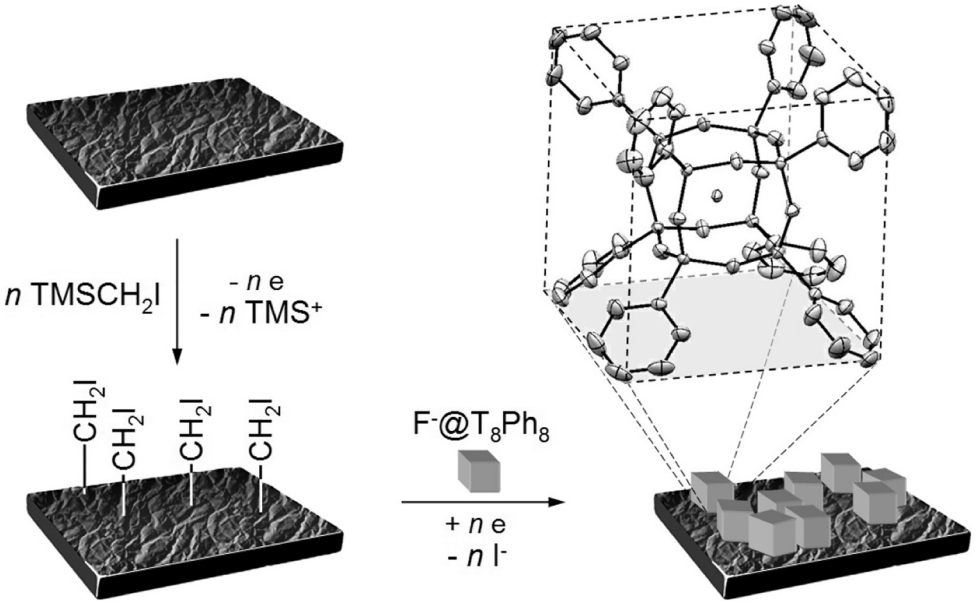

Scheme 1. Covalent immobilization of $F^-@Ph_8T_8$ on a GC interface (TBA^+ counter ions are not shown).

3. Results and discussion

Immobilization of $F^-@Ph_8T_8$ on a glassy carbon (GC) electrode was achieved in a two-step anodic/cathodic process (Scheme 1). First, 3–5 anodic cycles at a polished GC electrode were run in the range 1.2–2.2 V (Fig. 1 right, A) in a solution of $TMSCH_2I$ (3 mmol L^{-1} in CH_3CN/0.1 M $TBAPF_6$), leading to total passivation of the electrode surface by the grafted $–CH_2I$ groups, similar to the anodic grafting based on the elimination of TMS^+ reported recently [15,16]. This step is thought to involve two parallel processes: the oxidation of $TMSCH_2I$ to give a $^+CH_2I$ carbocation that adds to the aromatic sites on the GC electrode in a Friedel-Craft manner, and the oxidation of the C_{sp2} zones on the GC electrode to form a polyelectrophilic interface that substitutes the TMS moiety in an S_E2-like process. The EDS shows the presence of iodine atoms at an interface prepared in this way, and they remain attached to it even after intense ultrasonic cleaning.

The -CH_2I covered surface was then subjected to a slow cathodic scan from −1.0 V to −1.8 V at $\nu = 10$ mV s^{-1} (Fig. 1 left, B) in a solution of $F^-@Ph_8T_8[TBA^+]$ (3.5 mmol L^{-1} in CH_3CN/0.1 M $TBAPF_6$). After the first scan, the treated interface no longer showed any reduction signal of the pre-grafted -CH_2I groups. Electrochemical impedance spectroscopy (EIS) demonstrated the good conductivity of the $F^-@Ph_8T_8$-covered interface (Fig. 1, middle), unlike that capped with $–CH_2I$ (or $–CH_3$ that might be formed from further reduction of $–CH_2I$). A slow scan rate seems to be an important factor, allowing a longer time for appropriate arrangement of the initially grafted $F^-@Ph_8T_8$ on the surface in order to enable more than unitary attachment of any given $F^-@Ph_8T_8$ species and the formation of a compact grafted layer. At higher scan rates, $\nu > 50$–100 mV s^{-1}, the obtained layer has a higher R_{CT} because many $F^-@Ph_8T_8$ units are attached through a $–CH_2–$ linker by only one or two of the four phenyl substituents available for grafting, thus forming a less compact layer; the remaining unused CH_2I groups are reduced to CH_3.

Integration of the reduction current of the CH_2I-covered electrode (Fig. 1 left, B) yields the density of CH_2I groups on it (geometrical area) as $\Gamma = 1.23 \times 10^{-8}$ mol cm^{-2}. Taking into account free rotation about the C—C single bond, the projection of a grafted $CH_2\cdot$ radical ($r = 1.62$ Å) onto the electrode forms a circle of area ≈8.24 $Å^2$. On the other hand, the area of the projection of the zone around three phenyl carbon atoms suitable for radical attack by $CH_2\cdot$ (p- and 2 × m-) is ca. 18 $Å^2$ for each of the four “landing” phenyl groups of the Ph_8T_8 cage, i.e. covering more than twice the reach of a single $CH_2\cdot$ grafting site. In other words, the probability of multiple grafting of the Ph_8T_8 unit is quite high since each of the four Ph substituents of the silsesquioxane

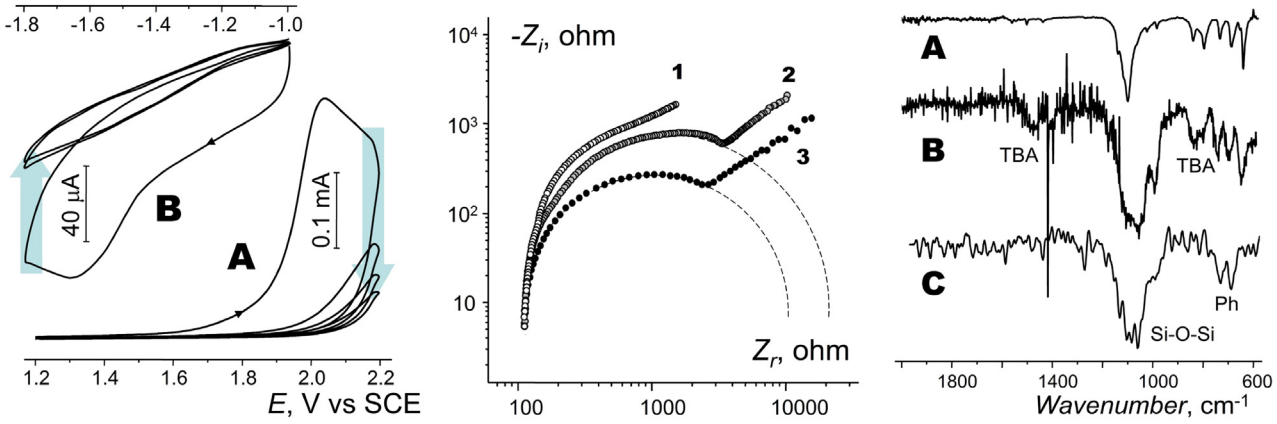

Fig. 1. Left: Two-step grafting of $F^-@Ph_8T_8$ onto a GC electrode and (middle) Nyquist plots of the reduction of chloranil on: (1) GC with grafted $F^-@Ph_8T_8$, (2) GC with grafted $–CH_2I$ and (3) $–CH_3$ layers. Right: FTIR reflectance spectra: (A) $F^-@Ph_8T_8[TBA]$; (B) GC interface with grafted $F^-@Ph_8T_8[TBA]$; (C) remaining Ph_8T_8 layer on the same electrode after 3 min contact with $LiClO_4$ solution.

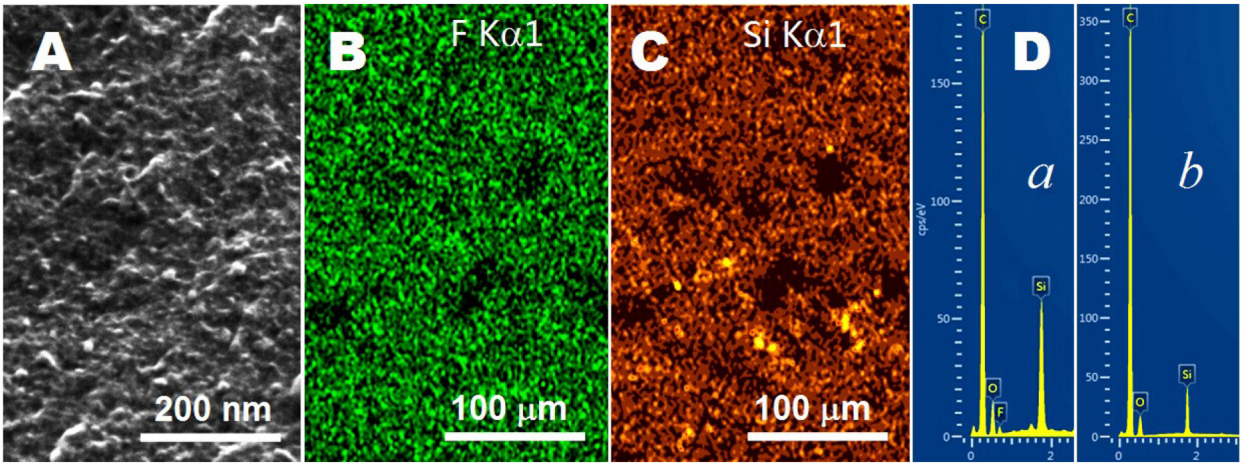

Fig. 2. (A) SEM of GC surface with immobilized $F^-@Ph_8T_8$[TBA] and its (B) F and (C) Si atom mapping. (D) EDS analysis of (*a*) a freshly grafted interface and (*b*) after its 5 min contact with 0.01 M $LiClO_4$ solution.

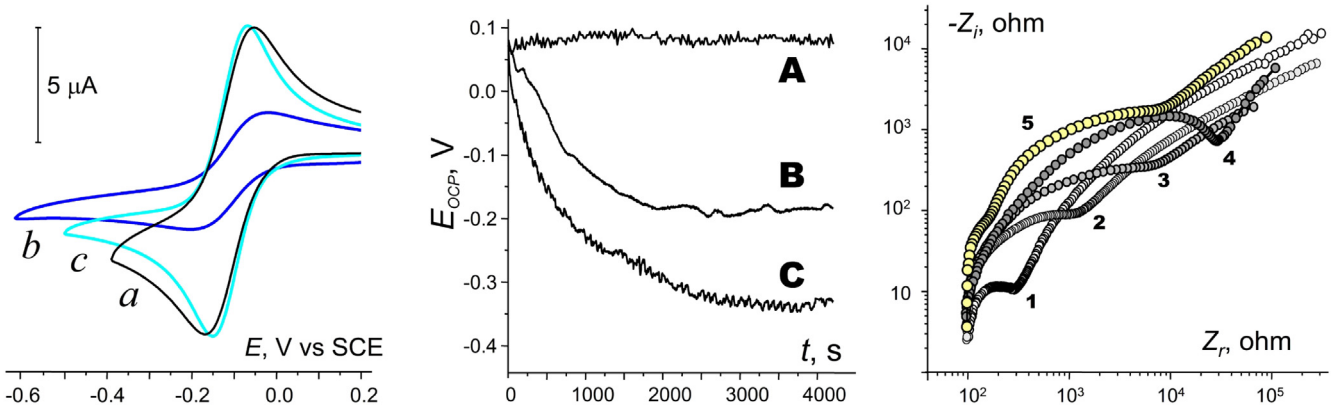

Fig. 3. Left: reduction of chloranil (2 mmol L^{-1}) in CH_3CN/0/1 M $TBAPF_6$. Voltammetry at a GC electrode with grafted: (a) $F^-@Ph_8T_8$ units attached by the $–CH_2–$ linker(s), (b) emptied Ph_8T_8 cage and (c) naked GC for comparison. Middle: Open circuit *E* – t plots for a $F^-@Ph_8T_8$–grafted GC electrode in CH_3CN/0.1 M $TBAPF_6$ (A). Same electrode, upon addition of (B) HCl (0.01 M) or (C) $LiClO_4$ (0.01 M). Right: Nyquist plots for the reduction of chloranil (2 mmol L^{-1}) at the $F^-@Ph_8T_8$–grafted electrode after its contact with CH_3CN/0.01 M $LiClO_4$ for (1) 10 s, (2) 1 min, (3) 3 min and (4) 35 min. (5) GC electrode with grafted empty-cage Ph_8T_8 octaphenylsilsesquioxane. Note several structure-related time constants.

approaching the interface covered with CH_2I groups will find at least two anchoring points on it.

The EDS Si/F mapping of the resulting $F^-@Ph_8T_8$-modified GC surface (Fig. 2A–C) shows a quite homogeneous distribution of grafted silsesquioxane units on the surface.

The affinity of the non-nucleophilic anion $F^-@Ph_8T_8$ for the GC surface seems to be even higher than that of the ClO_4^- anion since when using $TBAClO_4$ in place of $TBAPF_6$, a similar interface was obtained. Unlike diazonium grafting, the immobilization of $F^-@Ph_8T_8$ units using $TMSCH_2I$ exclusively yields a monolayer because the grafting only occurs at the $-CH_2I$ pre-coated interface, trapping the species that come into contact with it from near to the electrode solution layer; once the CH_2-Ph linkage is formed, the site is deactivated for further grafting. The resulting ionic interface is stable in air and over time, but upon exposure to solutions containing Li^+ or H^+ ions (Fig. 3 left, *a* and *b*, respectively), open circuit potential (OCP) measurements show its rapid evolution caused by extraction of the encapsulated fluoride anion from inside the Ph_8T_8 cage (Fig. 3, middle). The time it takes the $F^-@Ph_8T_8$ interface to release all its fluoride anions is quite similar for Li^+ and H^+ (as 0.01 M solutions). After all the F^- ions have left the immobilized $F^-@Ph_8T_8$ layer, EDS analysis shows that now only O and Si atoms are present at this interface (Fig. 2D). The R_{CT} of the remaining empty-cage Ph_8T_8 electrode coverage, determined by EIS, is much higher than that of the original ionic layer and is practically the same as that of surfaces grafted with hollow Ph_8T_8 silsesquioxane using a similar procedure (Fig. 3, right).

4. Conclusion

An ambifunctional commercially available "glue" reagent $TMSCH_2I$ was used in a new approach to combined anodic/cathodic grafting of a complex aromatic-organosilicon anionic cage structure to glassy carbon. This system can be used to detect Li^+ and H^+ ions or as a solid support for stabilizing/handling highly electrophilic cations. Seen more generally, electrochemical immobilization using $TMSCH_2I$ is a convenient and simple method for methylene linking of two (poly)aromatic units. This method does not require any preliminary chemical treatment of the substrates, which is necessary in other grafting methods in order to provide them with a functional anchoring group that would make possible their electrografting. Further work using this method to prepare flexible layered carbonaceous materials with on-demand interstitial distances is currently underway.

Acknowledgement

The authors warmly thank Prof. J. Simonet for stimulating discussions on surface modification. A.F. is grateful to the PHC OSMOSE program #39669QC for the travel grant and M.S. acknowledges support from the Russian Science Foundation, grant #17-73-20281.

References

[1] S. Alegret, A. Merkoci (Eds.), Electrochemical Sensor Analysis, Elsevier, 2007.
[2] A.R. Bassindale, M. Pourny, P.G. Taylor, M.B. Hursthouse, M.E. Light, Fluoride-ion encapsulation within a silsesquioxane cage, Angew. Chem. Int. Ed. 42 (2003) 3488–3489.
[3] A.R. Bassindale, D.J. Parker, M. Pourny, P.G. Taylor, P.N. Horton, M.B. Hursthouse, Fluoride ion entrapment in octasilsesquioxane cages as models for ion entrapment in zeolites. Further examples, X-ray crystal structure studies, and investigations into how and why they may be formed, Organometallics 23 (2004) 4400–4405.
[4] M. Syroeshkin, Y. Wang, M. Dieng, V. Gul'tyai, V. Jouikov, Octaorgano silsesquioxanes with encapsulated fluoride anion, TBA(F^-@T_8), as a new class of non-coordinating non-nucleophilic supporting electrolytes, ECS Trans. 45 (30) (2013) 29–38.
[5] J. Simonet, V. Jouikov, 9-Fluorenyl radical: electrochemical generation and cathodic immobilization at solid interfaces, Electrochem. Commun. 13 (3) (2011) 254–257.
[6] Y. El Aziz, P.G. Taylor, A.R. Bassindale, S.J. Coles, M.B. Pitak, Synthesis and structures of novel molecular ionic compounds based on encapsulation of anions and cations, Organometallics 35 (24) (2016) 4004–4013.
[7] J. Pinson, F. Podvorica, Attachment of organic layers to conductive or semi-conductive surfaces by reduction of diazonium salts, Chem. Soc. Rev. 34 (2005) 429.
[8] D. Bélanger, J. Pinson, Electrografting: a powerful method for surface modification, Chem. Soc. Rev. 40 (2011) 3995.
[9] F.I. Podvorica, Non-diazonium organic and organometallic coupling agents for surface modification, Aryl Diazonium Salts, Wiley-VCH, Ed. M. Chehini, 2012, p. 255.
[10] C.S.J.N. O'Donoghue, G. Fomo, T. Nyokong, Electrode modification using alkyne manganese phthalocyanine and click chemistry for electrocatalysis, Electroanalysis 28 (12) (2016) 3019–3027.
[11] W. Laure, K. De Bruycker, P. Espeel, D. Fournier, P. Woisel, F.E. Du Prez, J. Lyskawa, Ultrafast tailoring of carbon surfaces via electrochemically attached triazolinediones, Langmuir 34 (7) (2018) 2397–2402.
[12] S. Nagendiran, M. Alagar, I. Hamerton, Octasilsesquioxane-reinforced DGEBA and TGDDM epoxy nanocomposites: characterization of thermal, dielectric and morphological properties, Acta Mater. 58 (2010) 3345–3356.
[13] S.E. Anderson, D.J. Bodzin, T.S. Haddad, J.A. Boatz, J.M. Mabry, C. Mitchell, M.T. Bowers, Structural investigation of encapsulated fluoride in polyhedral oligomeric silsesquioxane cages using ion mobility mass spectrometry and molecular mechanics, Chem. Mater. 20 (2008) 4299–4309.
[14] M.Z. Asuncion, R.M. Laine, Fluoride rearrangement reactions of polyphenyl- and polyvinylsilsesquioxanes as a facile route to mixed functional phenyl, vinyl T_{10} and T_{12} silsesquioxanes, J. Am. Chem. Soc. 132 (2010) 3723–3736.
[15] V. Jouikov, J. Simonet, Efficient anodic allylation and benzylation of carbons using allyl and benzyl trimethylsilanes, Langmuir 29 (2013) 5556–5562.
[16] V. Jouikov, J. Simonet, An innovative anodic approach for efficient immobilization of an acetylenic triple bond via silicon–carbon bond scission, Electrochem. Commun. 93 (2018) 49–52.
[17] PowerSuite v. 2.58, PAR - Advanced Measurement Technology, (2003).

Novel R_3M (M = Si, Ge) substituted furan and thiophene-derived aldimines: synthesis, electrochemistry and biological activity

Jana Spura[1], Amel Farhati[2], Vitalijs Romanovs[1*], Artyom Borodulin[1], Sergejs Belakovs[1], Juris Popelis[1], Irina Shestakova[1], Mohamed Dammak[2] and Viatcheslav Jouikov[3*]

[1] Latvian Institute of Organic Synthesis, Aizkraukles 21, Riga, Latvia
[2] University of Sfax, Faculty of Sciences, 3000 BP 1171 Sfax, Tunisia
[3] UMR 6226 ISCR, University of Rennes I, 35042 Rennes, France

Abstract

New furan and thiophene derivatives of aldimines *o*-HO-C_6H_4N=CHC_4H_4X(R) (X = O, S; R = H, $SiMe_3$, $SiEt_3$, $GeMe_3$, $GeEt_3$) were synthesized by condensation of *o*-aminophenol with the substituted aldehyde precursor, and their structure, electrochemical reduction/oxidation (in CH_3CN/0.1 M Bu_4NPF_6), frontier orbital energies and cytotoxicity have been studied. Electrochemical redox potentials E_p of these new compounds show good correlation with the corresponding orbital energies and the difference E_p^{ox}–E_p^{red} corresponds well to their orbital hardness. The pronounced cytotoxicity of these new compounds can be modulated by the Me_3M group in the heterocyclic moiety, providing (M = Si) more than 50-fold increase in IC_{50} compared to the non-substituted derivative. The opposite trends were found: while $SiMe_3$ group decreases toxicity, $GeMe_3$ increases it and *vice versa*.

Résumé

Les nouveaux aldimines *o*-HO-C_6H_4N=CHC_4H_4X(R) (X = O, S; R = H, $SiMe_3$, $SiEt_3$, $GeMe_3$, $GeEt_3$), dérivés du furanne et du thiophène, ont été synthetisé par la condensation d'*o*-aminophenol avec un précurseur aldéhyde substitué ; la structure, la réduction et l'oxydation électrochimiques (dans CH_3CN/0.1 M Bu_4NPF_6), les énergies des orbitales frontières et la cytotoxicité de ces composés ont été etudiés. Les potentiels redox électrochimiques E_p de ces composés montrent une bonne corrélation avec les énergies orbitalaires correspondantes et la différence E_p^{ox}–E_p^{red} correspond bien à leur dureté orbitalaire. La cytotoxicité prononcée de ces nouveaux composés peut être modulée par le groupement MMe_3 dans l'hétérocycle, résultant (M = Si) en augmentation d'IC_{50} par plus de 50 fois par rapport au dérivé non substitué. Les tendances opposées ont été trouvée pour la toxicité: alors que le groupe $SiMe_3$ la diminue, $GeMe_3$ l'augmente et *vice-versa*.

Keywords*:* Aldimines, azomethines, furan, thiophene, redox potentials, cytotoxicity

1. Introduction

Aldehyde-derived imides of the formula RCH=NR', aldimines, are Schiff bases well known in coordination chemistry as mixed-donor ligands [1,2]. However, their chemistry found

* Corresponding authors. Email: vitalijs@osi.lv, vjouikov@univ-rennes1.fr

a much larger use for regio and stereoselective reactions, for total synthesis [3], and in preparations of pharmaceutically valuable products [4]. Besides purely synthetic aspect, redox reactions of aldimines have also been studied, especially during the "golden age" of organic electrochemistry, polarography being then the main method [5-9].

On the other hand, furan and especially thiophene units are present in many drugs [10]; but - with its evidently important role in their bioactivity, - the latter evokes a serious concern about the toxicity of reactive metabolites arising from the oxidation of thiophene-containing biomolecules for humans and animals [11]. Oxidation of thiophenes with CYP isoenzymes family - CYP450 (cytochrome 450), CYP2C9 and others - mainly proceeds via S-oxidation and epoxidation, both processes activating α-position of the heterocycle and usually leading to an α-hydroxythiophene or a thiolactone. Blocking this site with a neutral, oxidation-stable group might improve the oxidative stability of such compounds and decrease their metabolitic toxicity. This idea is supported by the fact that such thiophene-containing drugs as Duloxetine, Rivaroxaban and others, in which both α-positions of thiophene unit are substituted, have no toxicity [12], while those with one non-substituted α-position (Methapyrilene, Suprofen, Thienilic acid, OSI-920 and others) are toxic [13-15].

Studying thermochemistry and redox properties using DFT calculations [16] proved efficient providing meaningful leads to bioactivity of thiophene drugs. Because redox properties and biological activity of substrates are often correlated, and knowing that the introduction of a silyl or germyl substituent might modulate it, we undertook the present study aiming to prepare several new aldimine derivatives of furan and thiophene (**1a-e** and **2a-e**) with silyl and germyl substituents and to consider their bioactivity along with the electrochemical properties supported by DFT modeling.

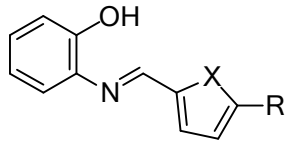

X = O; R = H (**1a**)	X = S; R = H (**2a**)
$SiMe_3$ (**1b**)	$SiMe_3$ (**2b**)
$GeMe_3$ (**1c**)	$GeMe_3$ (**2c**)
$SiEt_3$ (**1d**)	$SiEt_3$ (**2d**)
$GeEt_3$ (**1e**)	$GeEt_3$ (**2e**)

2. Experimental

Electrochemical measurements were carried out using a PAR 2373 potentiostat operating under PAR PowerSuite software, using a 5 ml glass electrochemical cell in the three-electrode mode. A glassy carbon (GC) disk (2 mm) sealed in a Pyrex tube was used as a working electrode; 3 × 50 mm GC rod served as a counter electrode. The working electrode was polished consecutively with Struers 2000 and 4000 paper before each run. All potentials, checked using Fc^+/Fc reversible couple (E^0 = 0.31 V vs. SCE [17]), are given vs. SCE.

DFT calculations (geometry optimization and frequency analysis) were performed using Gaussian 03W (release B.01) program [18] at B3LYP/Lanl2DZ//HF/6-31G level. Solvation in CH_3CN was accounted for using Tomasi PCM method [19]. All stationary points were found to be stable global minima as attested by the absence of negative vibration frequencies in harmonic frequency analysis. Scaling factor 0.98 was applied to B3LYP/Lanl2DZ calculated IR frequencies [20].

^1H and ^{13}C NMR spectra were recorded on a Varian-300 spectrometer (300 and 75 MHz, respectively) in $CDCl_3$, with TMS as internal standard for ^1H and ^{29}Si nuclei and using the residual solvent proton signal (77.05 ppm) for ^{13}C nuclei. Elemental analyses were performed on

a CARLO ERBA EA-1108 elemental analyzer. Thin-layer chromatography (TLC) was carried out on Merck silica gel 60 F254 plates. The mass-spectra were recorded under electron impact conditions on GC-MS Agilent Technologies 7890 GC system with 5975C EI/CI MSD (70 eV) and a capillary column HP-5.

For X-ray analysis diffraction data were collected at −100°C on a Bruker-Nonius KappaCCD diffractometer using graphite monochromatic Mo-Kα radiation (λ = 0.71073 Å). The crystal structures of **2b** and **2c** were solved by direct methods and refined by full-matrix least squares. All non-hydrogen atoms were refined in anisotropic approximation. Crystal data for **2b**: monoclinic: a = 6.6387(2), b = 13.4384(5), c = 16.7790(7) Å, β = 91.286(2)°; V = 1496.5(1) Å^3, Z = 4, μ = 0.285 mm^{-1}, Dcalc = 1.222 g·cm^{-3}; space group is $P2_1/n$. Crystal data for **2c**: monoclinic; a = 6.6635(2), b = 13.4717(3), c = 16.8383(4) Å, β = 91.045(1)°; V = 1511.30(7) Å^3, Z = 4, μ = 2.153 mm^{-1}, Dcalc = 1.406 g·cm^{-3}; space group is $P2_1/n$. For further details, see crystallographic data for **2b** and **2c** deposited at the Cambridge Crystallographic Data Centre as Supplementary Publications Numbers CCDC 1870490 (for **2b**) and CCDC 1870491 (for **2c**). Copies of the data can be obtained, free of charge, on application to CCDC, 12 Union Road, Cambridge CB2 1EZ, UK.

2-[2-furylmethylenamino]-phenol (1a). Furan-2-carbaldehyde (0.25 g, 2.3 mmol) and 2-aminophenol (0.22 g, 2.3 mmol) were placed in a round-bottomed flask equipped with reflux condenser, then benzene (2 mL) was added and the solution was refluxed for 4 hours. The reaction was monitored by TLC (PE(petroleum ether)/Et_2O, 10:0.1). After cooling down the solvent was evaporated, the residue was dissolved in diethyl ether and dried over $MgSO_4$. The obtained crude product was recrystallized from hexane affording 0.32 g (74%) of pure **1a** as a brown solid with melting point 62-63 °C (lit. m.p. [21]).
^{1}H NMR (300 MHz, $CDCl_3$), δ, ppm (J, Hz): 6.45 (m, 1H, J = 2.0 Hz); 6.83-7.3 (m, 6H); 7.52 (d, 1H, J = 2.0 Hz, CH_2-$\underline{CH_3}$); 8.4 (s, 1H).

2-[(5-trimethylsilyl-2-furyl)methylenamino]-phenol (1b) was prepared the same way as **1a**, using 5-trimethylsilyl-furan-2-carbaldehyde. The reaction mixture was stirred in ethanol at room temperature for 14 hours. Recrystallization of the crude product from hexane provided 0.19 g (71%) of pure **1b** as a yellow solid. M.p. 91-92°C.
^{1}H NMR spectrum, (300 MHz, $CDCl_3$), δ, ppm (J, Hz): 0.31 (s, 9H, Si-CH_3); 6.78-6.82 (m, 1H); 6.87-6.94 (m, 2H); 7.02-7.13 (m, 2H); 7.16-7.17 (d, 1H); 8.78 (s, 1H); 0.95 (s, 1H, OH). ^{13}C NMR spectrum, (75 MHz, $CDCl_3$), δ, ppm: ^{13}C NMR (75 MHz, $CDCl_3$), δ, ppm: -1.77; 115.08; 115.67; 115.73; 119.94; 121.71; 128.67; 135.77; 145.77; 152.34; 156.12; 165.58. ^{29}Si NMR (80 MHz, $CDCl_3$), δ, ppm: -9.55. MS (EI, 70 eV), m/z (I_{rel}, %): 259 $[M]^+$ (58); 231 (100); 216 (24); 186 (21); 150 (18); 73 (34); 28 (17). Anal. Calcd ($C_{14}H_{17}NO_2Si$), %: C 64.82; H 6.60; N 5.40. Found, %: C, 64.70; H 6.60; N 5.33.

2-[(5-trimethylgermyl-2-furyl)methylenamino]-phenol (1c) was prepared as described above for **1a**, using 5-trimethylgermyl-furan-2-carbaldehyde. The reaction mixture was stirred in ethanol at room temperature for 4.5 hours. The obtained crude product was recrystallized from hexane affording 0.15 g (66%) of pure **1c** as a light yellow solid, m.p. 94-96 °C.
^{1}H NMR (300 MHz, $CDCl_3$), δ, ppm (J, Hz): 0.48 (s, 9H, Ge-CH_3); 6.67-6.68 (d, 1H, J=3.3 Hz, H-3); 6.86-6.90 (m, 1H), 6.98-7.02 (m, 2H); 7.14-7.23 (m, 2H); 7.33 (ps, 1H, C-OH); 8.51 (s,

1H). ^{13}C NMR (75 MHz, $CDCl_3$), δ, ppm: -1.88; 114.97; 115.56; 116.09; 119.97; 120.25; 128.59; 135.81; 144.91; 152.34; 155.96; 165.60. MS (EI, 70 eV), *m/z* (I_{rel}, %): 305 $[M]^+$ (23); 277 (31); 186 (100); 158 (22); 119 (14); 28 (55). Anal. Calcd ($C_{14}H_{17}GeNO_2$), %: C 55.32; H 5.64; N 4.61. Found, %: C 55.54; H 5.66; N 4.47.

2-[(5-triethylsilyl-2-furyl)methyleneamino]-phenol (**1d**). 5-Triethylsilylfuran-2-carbaldehyde (0.43 g, 2.0 mmol) was added to a suspension of 2-aminophenol (0.22 g, 2.0 mmol) in ethanol (10 mL) and the resulting solution was stirred for 4.5 hours at room temperature. The reaction was monitored by TLC (PE/Et_2O, 10:0.1). After evaporation of ethanol, the residue was treated with toluene and then concentrated to remove any traces of water. The recrystallization of the crude product from hexane gave pure **1d** as a brown solid (0.42 g, 69%). M.p. 49-51°C.
^{1}H NMR (400 MHz, $CDCl_3$, δ, ppm): 0.80-0.89 (m, 6H, Si-CH_2), 1.00-1.01 (m, 9H, Si-CH_2CH_3), 6.86-6.91 (m, 1H), 6.98-7.0 (m, 1H), 7.14-7.18 (m, 2H), 7.65-7.28 (m, 2H), 7.55-7.56 (d, 2H), 8.79 (s, 1H). ^{13}C NMR (75 MHz, $CDCl_3$, δ, ppm): 4.20; 7.26; 114.96; 115.68; 119.99; 128.65; 133.24; 135.21; 135.28; 144.23; 147.29; 149.29; 152.24. ^{29}Si NMR (80 MHz, $CDCl_3$, δ, ppm): 0.98. MS, m/z (I, %): 317 (100), 288 (45), 260 (74), 232 (45), 170 (69), 116 (36), 28(87). Anal. Calcd ($C_{17}H_{23}NO_2Si$), %: C 67.73; H 7.69; N 4.64. Found, %: C 67.46; H 7.69; N 4.57.

2-[(5-triethylgermyl-2-furyl)methyleneamino]phenol (1e) was synthesized similarly to **1e**, using 5-triethylgermylfuran-2-carbaldehyde and a prolonged (12 hrs) stirring. Pure **1e** was obtained as a yellow solid (0.19 g, 66%). M.p. 64-65 °C.
^{1}H NMR (400 MHz, $CDCl_3$, δ, ppm): 1.06-1.16 (m, 15H, Si-CH_2CH_3); 6.83-6.93 (m, 3H); 7.11-7.17 (m, 1H); 7.21-7.23 (m, 1H); 7.38-7.41 (m, 1H); 7.84 (s, 1H); 8,69 (s, 1H). ^{13}C NMR (75 MHz, $CDCl_3$, δ, ppm): 4.44; 8.84; 114.88; 115.45; 115.72; 119.94; 121.41; 128.54; 135.71; 135.73; 144.80; 152.36; 156.16. MS, m/z (I, %): 347 (19), 318 (37), 290 (24), 260 (19), 186 (100), 131 (16), 28(89). Anal. Calcd ($C_{17}H_{23}GeNO_2$), %: C 59.01; H, 6.70; N, 4.04. Found, %: C 59.13; H 6.71; N 3.97.

2-[2-thienylmethylenamino]-phenol (2a) was prepared as described above for **1a**, using thiophene-2-carbaldehyde. The reaction mixture was refluxed for 4 hours. The obtained crude product was recrystallized from hexane affording 0.38 g (55%) of pure **2a** as a brown solid, m.p. 78-79 °C.
^{1}H NMR (300 MHz, $CDCl_3$), δ, ppm (*J*, Hz): 6.88-6.94 (m, 1H); 7.00-7.04 (m, 1H); 7.15-7.23 (m, 3H); 7.28-7.31 (m, 1H);7.52 (m, 2H); 8.8 (s, 1H). ^{13}C NMR (75 MHz, $CDCl_3$), δ, ppm: 115.02; 115.70; 120.04; 127.95; 128.81; 130.70; 132.47; 135.02; 142.88; 149.67; 152.22. MS (EI, 70 eV), *m/z* (I_{rel}, %): 203 $[M]^+$ (100); 170 (12); 120 (31); 110 (18); 65 (15); 28 (23). Anal. Calcd ($C_{11}H_9NOS$), %: C 65.00; H 4.46; N 6.89; S 15.77. Found, %: C 65.00; H 4.46; N 6.83; S 15.66.

2-[(5-trimethylsilyl-2-thienyl)methylenamino]-phenol (2b) was prepared as described above for **1a**, using 5-trimethylsilyl-thiophene-2-carbaldehyde. The reaction mixture was stirred in ethanol at room temperature for 10 hours. Recrystallization from hexane afforded 0.18 g (69%) of pure **2b** as a light yellow solid. M.p. 89-91°C.
^{1}H NMR spectrum, (300 MHz, $CDCl_3$), δ, ppm (*J*, Hz): 0.37 (s, 9H, Si-CH_3); 6.87-6.91 (m, 1H); 6.99-7.01 (m, 2H); 7.16-7.28 (m, 2H); 7.53-7.54 (d, 1H); 8.78 (s, 1H). ^{13}C NMR (75 MHz,

$CDCl_3$), δ, ppm: -0.32; 114.96; 115.64; 119.99; 128.69; 133.26; 134.49; 135.18; 147.26; 147.56; 149.24; 152.24. ^{29}Si NMR (80 MHz, $CDCl_3$), δ, ppm: -5.54. MS (EI, 70 eV), *m/z* (I_{rel}, %): 275 $[M]^+$ (100); 260 (23); 202 (15); 170 (67); 141 (82); 120 (18); 73 (29); 28(87). Anal. Calcd ($C_{14}H_{17}NOSSi$), %: C 61.14; H 6.23; N 5.09; S 1166. Found, %: C 61.03; H 6.26; N 4.98; S 11.63.

2-[(5-trimethylgermyl-2-thienyl)methylenamino]-phenol (2c) was prepared as described for **1a**, using 5-trimethylgermyl-thiophene-2-carbaldehyde. The reaction mixture was stirred in ethanol at room temperature for 8 hours. Pure **2c** (0.21 g, 63%) was obtained as a light yellow solid with m.p. 88-89°C.
^{1}H NMR (300 MHz, $CDCl_3$), δ, ppm (*J*, Hz): 0.51 (s, 9H, Ge-CH_3); 6.86-6.90 (m, 1H); 6.98-7.02 (m, 1H); 7.14-7.28 (m, 3H); 7.53-7.54 (d, 1H); 8.78 (s, 1H). ^{13}C NMR (75 MHz, $CDCl_3$), δ, ppm: -0.59; 114.93; 115.65; 119.99; 128.59; 133.19; 133.39; 135.29; 146.80; 149.18; 149.24; 152.24. MS (EI, 70 eV), *m/z* (I_{rel}, %): 320 $[M]^+$ (100); 305 (29); 277 (34); 186 (78); 158 (22); 119 (37); 28 (55). Anal. Calcd ($C_{14}H_{17}GeNOS$), %: C 52.54; H 5.36; N 4.38; S 10.02. Found, %: C 52.53; H 5.35; N 4.38; S 10.19.

2-[(5-triethylsilyl-2-thienyl)methyleneamino]-phenol (2d) was prepared similarly to **1d**, using 5-triethylsilylthiophene-2-carbaldehyde and stirring the mixture for 9 hours. After recrystallization from hexane, pure **2d** was obtained as a light yellow solid (0.26 g, 71%). M.p. 67-69 °C.
^{1}H NMR (400 MHz, $CDCl_3$, δ, ppm): 0.79-0.87 (m, 6H, Si-CH_2), 1.00-1.01 (m, 9H, Si-CH_2CH_3), 6.76-6.77 (m, 1H), 6.85-6.90 (m, 1H), 6.98-7.02 (m, 2H), 7.14-7.27 (m, 2H), 7.38 (s, 1H), 8.53 (s, 1H). ^{13}C NMR (75 MHz, $CDCl_3$, δ, ppm): 3.05; 7.23; 115.03; 115.36; 115.58; 119.94; 122.79; 128.67; 135.69; 144.99; 152.37; 156.28; 163.78. ^{29}Si NMR (80 MHz, $CDCl_3$, δ, ppm): -2.36. MS, m/z (I, %): 301 (88), 273 (90), 242 (100), 214 (69), 186 (45), 164 (36), 107(61), 59 (42). Anal. Calcd ($C_{17}H_{23}NOSSi$), %: C 64.30; H 7.30; N 4.41; S 10.10. Found, %: C 64.42; H 7.36; N 4.28; S 10.29.

2-[(5-triethylgermyl-2-thienyl)methyleneamino]phenol (2e). Using 5-triethylgermylthiophene -2-carbaldehyde as a starting compound in the same protocol as for **2c** and stirring the solution for 14 hours, pure **2e** was obtained after the recrystallization form hexane as a yellow solid with 69% yield (0.21 g). M.p. 68-69 °C.
^{1}H NMR (400 MHz, $CDCl_3$, δ, ppm): 1.05-1.15 (m, 15H, Si-CH_2CH_3), 6.85-6.90 (m, 1H), 6.98-7.01 (m, 1H), 7.13-7.19 (m, 3H), 7.24-7.27 (m, 1H), 7.54-7.56 (d, 1H), 8.78 (s, 1H). ^{13}C NMR (75 MHz, $CDCl_3$, δ, ppm): 5.43; 8.82; 114.91; 115.66, 119.99, 128.53; 133.22; 134.15; 135.38; 146.06; 146.85; 149.31; 152.20. MS, m/z (I, %): 363 (59), 334 (97), 306 (21), 276 (17), 202 (18), 170 (100), 139(49), 97 (43), 28 (91). Anal. Calcd ($C_{17}H_{23}GeNOS$), %: C 56.39; H 6.40; N 3.87; S 8.86. Found, %: C 56.48; H 6.36; N 3.78; S 8.97.

3. Results and Discussion

3.1 Synthetic approach

Aldimines **1a-e** and **2a-e** were prepared by condensation of 2-aminophenol with the corresponding aldehyde in refluxing benzene (Scheme 1). However, refluxing in this solvent

(even for 40 hrs) turned out to be poorly suitable for preparing trimethylsilyl(germyl)-substituted furan and thiophene aldimines: the aldehyde did not react completely and the attempts to recrystallize the product from the reaction mixture led to its decomposition. Changing the reaction conditions (stirring in ethanol at room temperature for 4.5–14 hours) allowed us to obtain trimethylsilyl(germyl)-substituted aldimines with 63–71% yields.

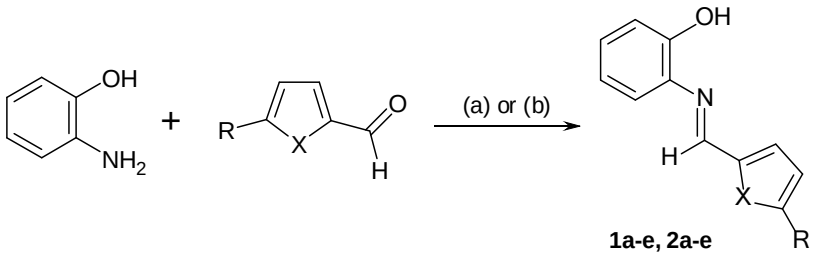

Scheme 1. Synthesis of aldimines **1a-e** and **2a-e.** (a) For **1a**, **2a**: benzene, 80 °C, (b) for **1b-e** and **2b-e**: EtOH, rt.

3.2 Structural features

The structure of the compounds **2b** and **2c** was confirmed by X-ray diffraction analysis (Figs 1, 2). The crystal structures of **2b** and **2c** are isomorphous. Their molecular structures are characterized by strong intramolecular hydrogen bonds of the OH···N type pointing the OH group towards the azomethine bridge. The corresponding lengths of this contact are 2.621(2) Å (H···N = 2.06(3) Å and ∠O-H···N = 128(2)º) for **2c** and 2.617(2) Å (H···N = 2.05(2) Å and ∠O-H···N = 124(2)º) for **2b**. In the crystal state, these hydrogen bonds are bifurcated forming additional OH···O type intermolecular bonds between the neighboring molecules. The lengths of these intermolecular bonds are 2.934(2) Å (H···O = 2.52(2) Å and ∠O-H···O = 114(2)º) for **2c** and 2.938(2) Å (H···O = 2.48(2) Å and ∠O-H···O = 115(2)º) for **2b**.

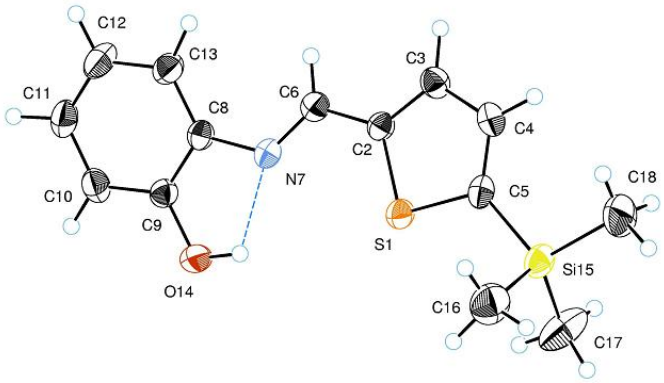

Figure 1. ORTEP structure of 2-[(5-trimethylsilyl-2-thienyl)methylenamino]phenol (**2b**). Thermal ellipsoids are shown with 50% probability. The intramolecular OH···N hydrogen bond is shown with dotted line. Selected geometrical parameters: N-C(6) = 1.279(4) Å, N-C(8) = 1.412(6) Å, C(6)-C(2) = 1.442(9) Å, Si-C(18) = 1.851(6) Å, Si-C(16) = 1.858(4)Å, ∠C(8)-N-C(6)-C(2) = 175.61º, ∠N-C(6)-C(2)-S = 1.07º, ∠S-C(5)-Si-C(18) = 179.76º.

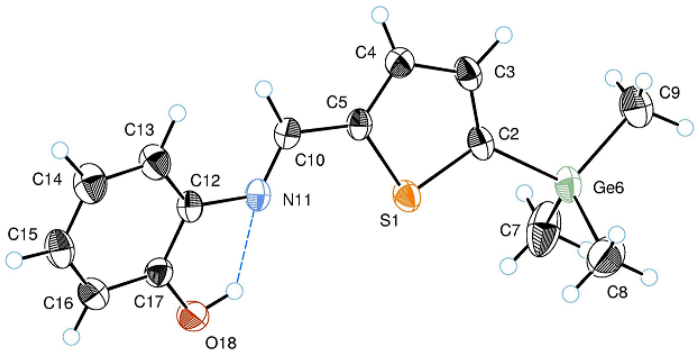

Figure 2. ORTEP drawing of 2-[(5-trimethylgermyl-2-thienyl)methylenamino]phenol (**2c**). Thermal ellipsoids are shown with 50% probability. The intramolecular OH···N hydrogen bond is shown with dotted line. Selected geometrical parameters: N-C(12) = 1.415(1) Å, N-C(10) = 1.272(8) Å, C(6)-C(2) = 1.443(6) Å, Ge-C(9) = 1.933(3) Å, Ge-C(7) = 1.937(3)Å, ∠C(12)-N(11)-C(10)-C(5) = 174.93º, ∠N-C(10)-C(5)-S = 1.89º, ∠S-C(2)-Ge-C(9) = 179.98º.

In both structures, the N=C azomethine fragment is not distorted (∠NC_6C_2 = 121.08º and ∠C_8NC_6 = 122.25º in **2b**, while in **2c** these angles are 120.85º and 122.28º, correspondingly) and is coplanar to the thiophene unit (dihedral angles ∠N-C-C-S are 1.07º and 1.89º for **2b** and **2c**, respectively). However, phenyl and thiophene rings are twisted with respect to each other by ca. 18º (the dihedral ∠$C_{13}C_8NC_6$ in **2b** and its equivalent in **2c** are 18.18º and 17.79º, respectively) which somewhat disturbs their ring-to-ring π-conjugation. In the absence of obvious electronic reasons for this, the energy causing this twist visibly arises form *ortho*-repulsion between the C-H protons of phenyl and azomethine units. In fact, though σ(C_3-H) and σ(C_6-H) bonds in **2b** are eclipsed and practically parallel (same for σ(C_{10}-H) and σ(C_4-H) in **2c**), they are quite distant (H···H = 2.715(2) Å (**2b**) and 2.681(7) Å (**2c**)), while the phenyl C_{13}-H and methine C_6-H protons are closer (H···H = 2.379(2) Å and 2.100(8) Å for **2b** and **2c**, respectively) forming an open 6-membered structure (Fig. 1 and 2).

Remarkably, the M-$C_{thienyl}$ bond in both **2b** (M = Si) and **2c** (M = Ge, Ge-C_2 = 1.946(9) Å) is longer than the three other M-C bonds, and one of these three M-C bonds (eclipsed M-Me,) is ca. 0.003-0.004 Å shorter that two others (e.g. Ge-C_9 = 1.933(3) Å and Ge-C_7 = 1.937(3) Å, Fig. 2). This feature attests to an additional π-$σ_{(C-M)}$-type hyperconjugation of the Me_3M groups with the heterocycle in both **2b** and **2c** which overcomes the repulsion energy of the eclipsed σ-bonds in the practically planar H-C(3)-C(2)-Ge-C(9) fragment (∠SC_2GeC_9 = 179.98º).

The structure of the synthesized aldimines was also confirmed by mass, ^{1}H NMR, ^{13}C NMR and ^{29}Si NMR (for **1b** and **2b**) spectroscopy.

3.3 Electrochemical study

Known electrochemical data on aldimines were obtained mostly in acid or basic media, at pH rarely met in biological systems [7,9,22]. In addition, these compounds are not stable under such conditions and in aqueous media with pH even moderately different form neutral their redox processes are complicated by acid-base interactions and are dependent, besides chemical structure, on different factors (concentration, proton activity, supporting electrolyte etc [8]). The redox reactions following first electron transfer (ET) usually produce highly reactive intermediates (ions or radical ions very improbably to be formed in biological processes [22]);

otherwise they concern secondary stable products resulting from the initial electron release/uptake. When R is a good leaving group, the reduction of the >C=N-R unit might result in the N-R bond scission leading to a corresponding nitrile [23,24] and an RH compound so as the immediate biological effect might be anticipated knowing the nature of these products. The oxidation of aldimines in aqueous solutions or in wet organic media involves the N=C bond cleavage as well, leading through the formation of a protonated anisidine to the corresponding aldehyde and the quinone imine [25]. Therefore, only first redox steps might be considered as characteristic of biological relevance of aldimines as such.

At a fixed R (*o*-C_6H_4OH), electron affinity and ionization of the π-system of aldimines are the prime factors in their redox activity [9], so we considered first redox potentials of the reaction series **1a-e** and **2a-e** and the energies of the frontier orbitals (FO) corresponding to these processes.

At a Pt electrode in CH_3CN/0.1 M Bu_4NPF_6, the voltammograms of **1a-e** and **2a-e** are irreversible and poorly reproducible because of electrode passivation. At a glassy carbon (GC) electrode, the curves were better shaped (Fig. 3) albeit some accompanying peaks appeared upon scanning because of the propensity of these compounds to adsorption and electropolymerization [26]. The oxidation potentials are close to those reported (in CH_2Cl_2/0.1 M Bu_4NClO_4) for structurally-related thiophene(furan) bis-substituted phenyl aldimines [27]. The i_p peak currents of both – oxidation and reduction – steps are diffusion-controlled as follows from their linearly dependence on concentration and on the scan rate ($i_p/Cv^{1/2}$ = const). The reduction peak half-widths ($\Delta E_{p\text{-}p/2} = E_p - E_{p/2}$, Table 1) are broadened in both series over 58 mV typical for electrochemically reversible processes [28]. Supposedly, this is not due to a slow electron transfer (ET) since the kinetic shift of the E_ps of **1a-e** and **2a-e** with the scan rate ($\Delta E_p/\Delta\ln(v) \cong$ 35-40 mV) remains close to 30 mV per decade of *v*, corresponding to a EC mechanism with fast first order reaction following ET [28]. This trend is also supported by somewhat larger oxidation peaks (higher $\Delta E_{p\text{-}p/2}$, Table 1) because of preferential adsorption of thiophene at anodic potentials [29]. The redox characteristics of **1a-e** and **2a-e** in reduction and oxidation processes are collected in Table 1.

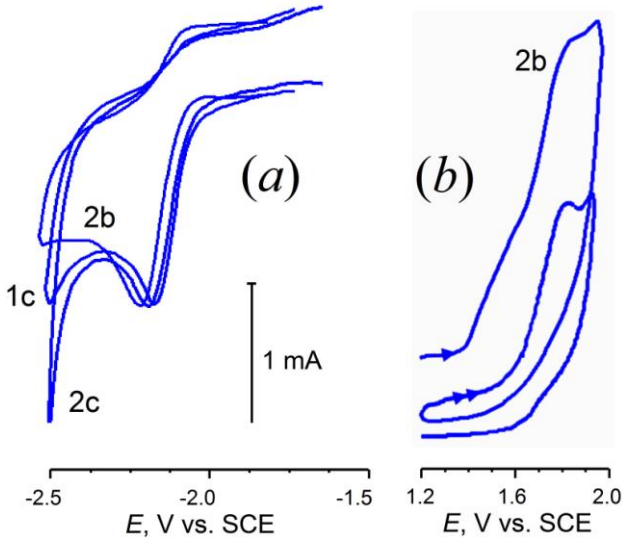

Figure 3. Voltammograms of (a) reduction of **1c, 2b** and **2c**, and (b) oxidation of **2b** (first and second cycles) in CH_3CN/0.1 M Bu_4NPF_6 at a GC disk electrode. Scan rate v = 0.2 V s^{-1}. T = 20 °C.

Table 1. Reduction and oxidation potentials E_p (V vs. SCE), peak half-widths ($\Delta E_{p\text{-}p/2}$, mV),[a] frontier orbital energies (ε, Δε, eV)[b] and dipole moments (μ, D)[b] of **1a-e** and **2a-e**

Cpd	*Reduction*			*Oxidation*			μ	ΔE_p [c]	Δε [d]
	E_p^{red}	$\Delta E_{p\text{-}p/2}$	$-\varepsilon_{LUMO}$	E_p^{ox}	$\Delta E_{p\text{-}p/2}$	$-\varepsilon_{HOMO}$			
1a	-2.169	75	2.327	1.879	95	6.019	6.22	4.048	3.693
1b	-2.149	76	2.160	1.756	88	5.722	4.06	3.905	3.562
1c	-2.140	84	2.136	1.761	90	5.702	4.07	3.901	3.566
1d	-2.142	80	2.128	1.753	85	5.689	4.01	3.895	3.561
1e	-2.138	76	2.100	1.752	80	5.664	4.02	2.890	3.563
2a	-2.185	89	2.371	1.834	>110	5.870	4.07	4.019	3.500
2b	-2.180	80	2.309	1.782	>130	5.778	4.22	3.962	3.468
2c	-2.168	75	2.285	1.803	90	5.759	4.29	3.971	3.474
1d	-2.168	72	2.274	1.783	80	5.744	4.28	3.469	3.469
1e	-2.166	78	2.248	1.767	82	5.722	4.38	3.933	3.474

[a] at GC electrode in CH_3CN/0.1 M Bu_4NPF_6; [b] from DFT B3LYP/Lanl2DZ//HF/6-31G calculations; [c] $\Delta E_p = E_p^{ox} - E_p^{red}$; [d] $\Delta\varepsilon = \varepsilon_{HOMO} - \varepsilon_{LUMO}$.

The E_ps of both processes are clearly affected by the nature of heteroaromatic unit at the methine carbon and by the substituent at its α-position, though the last effect is modest. Indeed, $GeMe_3$ group in aromatic systems exerts same polar substituent effect as H (i.e. $\sigma_p = 0$ [30]), while $SiMe_3$ acts as a weak donor ($\sigma_p = -0.07$) [30]. Of 2-furyl and 2-thienyl substituents, the former is slightly less acceptor ($\sigma_p = 0.02$ and 0.05, respectively [30]) though the whole effect is rather small. Similar trend is true for the additive inductive constants of these groups ($\sigma^* = 1.11$ and 1.28) [31]. Thus, the resulting influence of R in **1a-c** and **2a-c** is distinct but rather small to cause a dramatic differentiation in their redox properties.

These molecules are quite polar (dipole moment $\mu = 4.06\ldots6.22$ D), yet this parameter follows different trends in the series **1a-c** and **2a-c**. Interestingly, most polar derivatives **1a** and **2c** seem to have more pronounced biological activity (see §3.5).

3.4 DFT modeling

Experimental electrochemical quantity $E_p^{ox} - E_p^{red}$ ($E_0^{ox} - E_0^{red}$ in case of purely reversible processes) reflects the fundamental orbital quantity, the HOMO–LUMO energy difference,* which characterizes chemical "hardness" of a molecule [35]. Both quantities are directly linked to its donor-acceptor ability that can be considered in terms of nucleo/electrophilicity or acido-basicity [36,37], the parameters closely related to biological activity [38-39]. However, the comparison of the experimental redox data with orbital energies is only possible using right geometry for the FO energy calculations because the conjugation in planar systems **1a-e** and **2a-e** is very sensitive to structural factors. The (E)-form of **1a** is more favorable over its (Z)-form (with the planes of C_6H_4OH and furan units helix-wise twisted out of the common plane by strong *ortho*-repulsion, ΔG[**1a**(E) – **1a**(Z)] = -6.44 kcal mol^{-1} (DFT

* Strictly speaking, E_p is not an equivalent of E_0 since it is shifted with respect to E_0 by the ensuing chemical reaction ("kinetic shift") [28]. However, this shift is often constant or linear with E_0, so that using E_p instead of E_0 might often be a good approach; see [32-34].

B3LYP/Lanl2DZ), and this is the form which was actually formed, in agreement with X-ray data. Important intramolecular N···H interaction in **1a** stabilizes this system by 20.4 kcal mol^{-1} compared to a non-coordinated structure. On the potential energy curve of (E)-2-(furan-2-ylmethylenamino)phenol, three minima are marked. The form with σ-trans position of N and O(furan) atoms, where all three chelating centers (O, N, O) are pointed to the same direction while azomethine C-H bond is turned to the opposite side, corresponds to the global minimum in the gas phase and in CH_3CN solution; two other (E)-forms being local minima with higher energy (Fig. 4). Similar configuration is found to be the global minimum for **2a** as well.

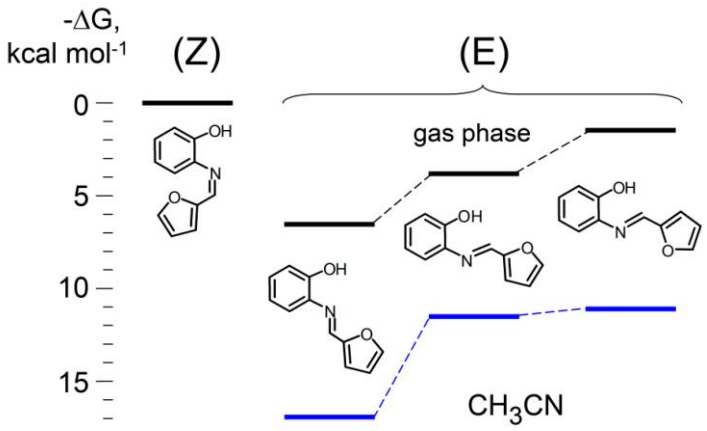

Figure 4. Relative free energies of formation of the different forms of 2-(furan-2-ylmethylenamino)-phenol **2a**. In blue: values in CH_3CN. From DFT B3LYP/Lanl2DZ (CPM) calculations.

This configuration is in agreement with the experimental IR spectra of **1a** and **2a**. A broad band at $\nu_{O\text{-}H}$ = 3000 cm^{-1} is due to the vibration of OH hydrogen involved into the intramolecular coordination with N atom [40]. Respectively, the $\nu_{C\text{-}O}$ band now appears at 1472 cm^{-1}, and characteristic Schiff base $\nu_{C=N}$ band [41] is shifted to lower frequencies (ν = 1634 cm^{-1}) because of N···H coordination (cf. X-ray structures of **2b** and **2c**, Fig. 1, 2). Methine C-H bond in **1a** and **2a** vibrates with practically similar frequency typical for this conformation ($\delta_{C\text{-}H}$ = 3035 cm^{-1}), which is well reproduced by DFT calculations (Fig. 5).

The frontier orbitals (FOs) (Fig. 6) are quite similar in the reaction series **1** and **2**, main difference arising from the orbital coefficients of O and S in the heteroaromatic rings. Remarkably, Me_3Si and Me_3Ge substituents do not strongly perturb these orbital features: neither Si nor Ge are directly involved in these FO, the substituents are mostly contributing through hyperconjugation of their M-C_{sp3} (M = Si, Ge) bonds with the π-electron system (Fig. 6) in agreement with what was observed by X-ray diffractometry (Fig. 1, 2).

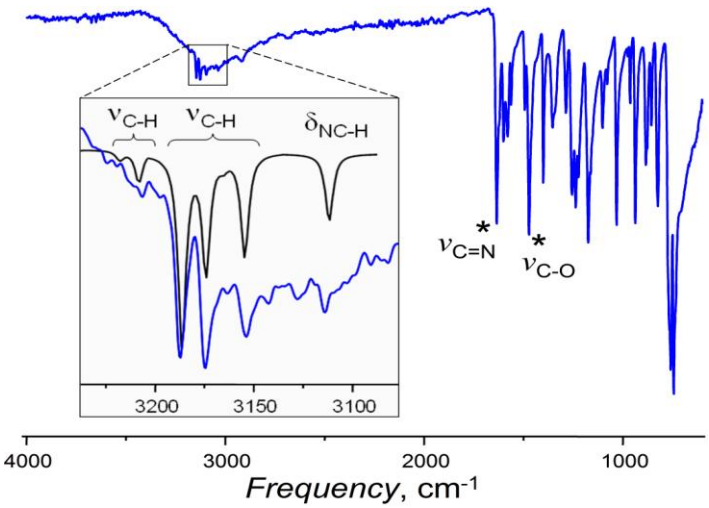

Figure 5. IR spectrum of **1a**. In the inset, appearing on the large $\nu_{O\text{-}H}$ band, are DFT-calculated (black) IR frequencies of aromatic C-H bonds in furan (left group) and phenol (right group), and of the methine (N=)C-H carbon-proton bond.

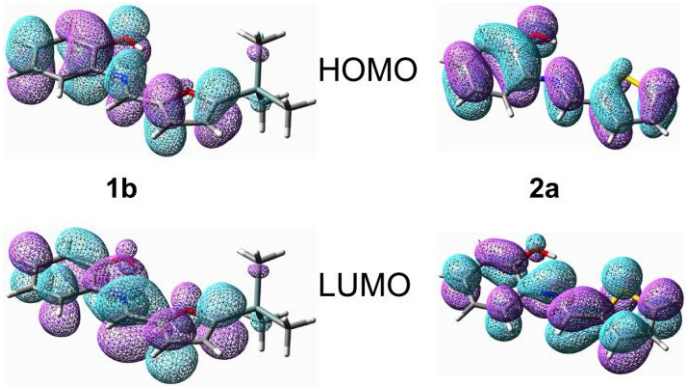

Figure 6. Redox-related frontier orbitals (HOMO and LUMO) of **1b** and **2a** (From DFT B3LYP/Lanl2DZ calculations).

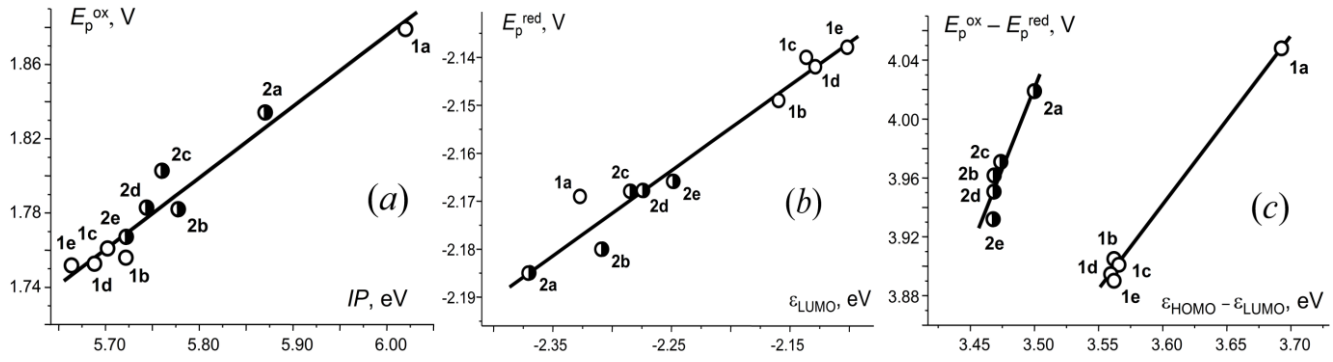

Figure 7. Correlations of (a) E_p^{ox} with first ionization potential (IP = $-\varepsilon_{HOMO}$); (c) E_p^{red} with LUMO energy; (c) the difference in first redox potentials ($E_p^{ox} - E_p^{red}$) with the $\varepsilon_{HOMO} - \varepsilon_{LUMO}$ difference.

Figure 7 thus shows the E_p^{ox} and E_p^{red} plotted against the corresponding FO energies, and that correlation of ($E_p^{ox} - E_p^{red}$) with the $\varepsilon_{HOMO} - \varepsilon_{LUMO}$ difference. In both families, **1a-e** and **2a-**

e, E_p^{ox} – IP and E_p^{red} – ε_{LUMO} are well correlated forming common plots though their less than unity slopes ($\Delta E_p^{ox}/\Delta IP$ = 0.38 and $\Delta E_p^{red}/\Delta\varepsilon_{LUMO}$ = 0.18) indicate strong influence of the chemical reaction following first ET on the experimental E_ps (large kinetic shift). Quite similar trends were previously found for furyl and thienyl nitrones and nitroethenes [32]. When considered in terms of orbital hardness, furyl and thienyl substituted aldimines form two different groups (Fig. 7, c). Interestingly, charge-based isotropic dipole moments μ of **1a-e** and **2a-e**, reflecting their polarity, are distinctly in line with each of the orbital energies, ε_{HOMO} and ε_{LUMO} (Table 1), but they loose the selectivity for their difference and are no more specific for properties correlations.

3.5 Cytotoxicity and toxicity

Aldimines and their derivatives possess a broad spectrum of biological activity, such as anti-bacterial and anti-cancer [42], anti-fungal (*Candida albicans* and *Aspergillus niger*) [4], anti-inflammatory, anti-virus, anti-pyretic [43], and a significant activity against *Staphylococcus aureus* and *epidermidis, Bacillus subtilis* and *cereus, Micrococcus luteus,* and *Escherichia coli*. Their complexes with metals (e.g. Cu, Ni, Zn) showed very good activity against leukemia cells (CEM-SS) [4].

The *in vitro* cytotoxicity of heteroaryl substituted aldimines **1a-e** and **2a-e** was investigated for two tumor lines, HT-1080 (human fibrosarcoma) and MG-22A (mouse hepatoma), and on normal mouse fibroblasts NIH 3T3 in order to determine the effect of the substituent at the 5-position and the type of heterocycle on antitumor activity. The results of experimental evaluation of the cytotoxic properties are presented in Table 2.

The aldimines **1a** and **1c** have high cytotoxic activity (IC_{50} 1-8 μg ml^{-1}) on both cancer cell lines, these compounds also have high cytotoxic effect on NIH 3T3 cells (IC_{50} 1-9 μg ml^{-1}). The introduction of Me_3M substituent to the heterocycle has a special effect in both O and S series. In furan series, the silylated aldimine **1b** generally shows a decrease in both cytotoxicity and toxicity. Its thiophene analogue **2b** shows better cytoselectivity: it has higher cytotoxicity on cancer cell line MG-22A (IC_{50} 6 μg ml^{-1}) than on HT-1080 (IC_{50} 26 μg ml^{-1}) but unlike other aldimines of this family this compound is very toxic (LD_{50} 4 mg kg^{-1}). Me_3Ge-substituted **2c** is more promising here as having practically similar cytotoxicity as non-substituted **2a** but with reduced toxicity. Aldimine **1d** has most pronounced cytotoxicity in these series for both HT-1080 and NIH 3T3 cells but at the same time it is quite toxic, LD_{50} < 60 mg·kg^{-1}. In contrast, its thiophene analogue **2d** is the less toxic (Table 1) although also less efficient against the two tumor lines and NIH 3T3. Et_3Ge-Substituted furan derivative **1e** has a good cytotoxicity towards NIH 3T3 at rather high LD_{50}, but it is less selective for HT-1080 and MG-22A tumor cells.

Remarkably, both Me_3Si derivatives, **1b** and **2b**, have lowest oxidation E_ps in the corresponding series (Table 1). However, while α-Me_3Si group promotes (for Me_3Si neighboring group effect, see e.g. [44]) the S-oxidation, similar to the oxidation by cytochrom CYP450 [16], the oxidation of the furan derivative is not O-centered and follows a different way. We venture to suppose that the acute toxicity of **2b** might be related to its easier metabolitic S-oxidation leading to toxic products [11,16]. Parent α-Me_3Ge group in **2c** is less conjugated with the π-system of the heterocycle because of the size mismatch of its more diffuse $\sigma_{(C\text{-}Ge)}$ orbitals responsible for the electronic effects, so probably its overall action results from different factors (solubility, coordination of Ge with biological phosphates etc). Interestingly, when Me_3Si group increases the toxicity, Me_3Ge group induces the opposite trend and *vice versa*.

Overall, aldimines **1a**, **2a** and **2c** seem to have more advantageous combination of biological properties providing good leads for the further development in these reaction series.

Table 2. *In vitro* cytotoxicity (IC_{50}) and toxicity (LD_{50}) of aldimines **1a-e** and **2a-e**

Compound	IC_{50}, μg ml^{-1}			LD_{50}, $mg \cdot kg^{-1}$
	HT-1080 MTT*	MG-22A MTT	NIH 3T3 NR	
1a	2	1	9	187
1b	>100	30	11	259
1c	3	8	1	91
1d	0.2	2	<0.3	<60
1e	24	21	5	232
2a	10	8	12	144
2b	26	6	193	4
2c	18	12	15	192
2d	56	12	43	483
2e	21	25	17	398

* Coloration indicators: MTT = 3-(4,5-dimethylthiazol-2-yl)-2,5-diphenyl-2H-tetrazolium bromide, NR = neutral red.

To conclude, new aldimines, derivatives of *o*-aminophenol, with furane and thiofene substituents (C_4H_4X, X = H, $SiAlk_3$, $GeAlk_3$, with Alk = Me, Et) were synthesized through a simple procedure condensing the aniline with the corresponding precursor aldehyde. The structure of these new products as well as redox properties in CH_3CN/0.1 M Bu_4NPF_6, their frontier orbital energies, cytotoxicity and toxicity have been considered. Their electrochemical redox potentials E_p show good correlation with the related orbital energies and the difference $E_p^{ox} - E_p^{red}$ corresponds well to the orbital hardness of these compounds. Me_3Si and Me_3Ge substitution of the heterocycle facilitates the oxidation of the corresponding molecules (promoting their oxidative metabolism), and - though not dramatically - alter their redox properties. However, remarkably reducing their orbital hardness, Me_3M substitution can also substantially affect solubility and hydro(phobicity/philicity) and hydrogen-bonding ability of these molecules. Steric hindrance of both Me_3M groups is relatively small because of longer C-Si and C-Ge bonds compared to C-C; this same feature accounts for attenuating their electronic interaction (hyperconjugation) with the aldimine π-system, especially for Me_3Ge group. To the overall effect of this latter, additional factors add such as more diffuse conjugating $\sigma_{(C\text{-}Ge)}$ orbital and longer Ge-C(H_3) bonds making Ge more available for external coordination and nucleophilic interactions. With this, both substituents distinctly modulate the biological properties and have important consequences for metabolic processes. Further works in this field are in progress.

Acknowledgements

The authors gratefully acknowledge the support of this research by Latvian Council for Science (Project 225/2012) and from PHC OSMOSE #39669QC.

References

[1] B.O. West, Chemistry of coordination compounds of Schiff bases, Ch. 13. In: New pathways in inorganic chemistry, Eds. E.A.V. Ebsworth, A.G. Madock, A.G. Shappe, Cambridge University Press, London, (1968) 303.
[2] R.K. Pardeshi, Coordination chemistry of Schiff bases: metal-ligand complexes, Lambert Academic Publishing, (2016).
[3] Carbon-Nitrogen double bonds, Patai's chemistry of functional groups, Ed. S. Patai, John Wiley & Sons, Inc., NY, (1970).
[4] R. Sahu, D.S. Thakur, P. Kashyap, Int. J. Pharm. Sci. Nanotechnol., 5/3 (2012) 1757-1764.
[5] L. Eberson, K. Nyberg, In: Enyclopedia of electrochemistry of the elements, Vol. 12, Eds Bard, A.J.; Lund, H.; Marcel Dekker, NY, (1978) 261-238.
[6] Y.P. Kitaev, T.V. Troepolskaya, Polarographic reduction of azomethine compounds, In: Progress in Electrochemistry of organic compounds 1, Ed. A.N. Frumkin, A.B. Ershler, Plenum Publishing Co., Ltd, NY, (1971) 43-83.
[7] T.V. Troepolskaya, G.K. Budnikov, Electrochemistry of azomethines, Nauka, Moscow, (1989) 216.
[8] H. Lund, Electrochemistry of the carbon-nitrogen double bonds, Ch 11, In: Carbon-Nitrogen Double Bonds, Patai's Chemistry of Functional Groups, Ed. Patai, S. John Wiley & Sons, Inc., NY, (1970) 505.
[9] H. Lund, Reduction of azomethine compounds, In: Organic Electrochemistry; Lund, H.; Hammerich, O., Eds., Marcel Dekker: New York, 4th ed., (2001) 435.
[10] M. Krátký, J. Vinsova, Curr. Topics Medicin. Chem., 26 (2016) 2921-2952.
[11] D. Gramec, L. P. Masic, M. S. Dolenc, Chem. Res. Toxicol. 27 (2014) 1344-1358.
[12] C. Weinz, T. Schwarz, D. Kubitza, W. Mueck, D. Lang, Drug Metab. Dispos. 37 (2009) 1056-1064.
[13] E. E. Graham, R. J. Walsh, C. M. Hirst, J. L. Maggs, S. Martin, M. J. Wild, I. D. Wilson, J. R. Harding, J. G. Kenna, R. M. Peter, D. P. Williams, B. K. Park, J. Pharmacol. Exp. Ther. 326 (2008) 657-671.
[14] J.P. O'Donnell, D.K. Dalvie, A.S. Kalgutkar, R.S. Obach, Drug Metab. Dispos. 31 (2003) 1369-1377.
[15] C. Medower, L. Wen, W.W. Johnson, Chem. Res. Toxicol. 21 (2008) 1570-1577.
[16] C.K. Jaladanki, N. Taxak, R.A. Varikoti, P.V. Bharatam, Chem. Res. Toxicol., 28*/12* (2015) 2364-2376.
[17] C.K. Mann, K.K. Barnes, Electrochemical Reactions in Nonaqueous Systems, Marcel Dekker, NY, (1970) 403.
[18] M. J. Frisch, G. W. Trucks, H. B. Schlegel, G. E. Scuseria, M. A. Robb, J. R. Cheeseman, J. A. Montgomery Jr., T. Vreven, K. N. Kudin, J. C. Burant, J. M. Millam, S. S. Iyengar, J. Tomasi, V. Barone, B. Mennucci, M. Cossi, G. Scalmani, N. Rega, G. A. Petersson, H. Nakatsuji, M. Hada, M. Ehara, K. Toyota, R. Fukuda, J. Hasegawa, M. Ishida, T. Nakajima, Y. Honda, O. Kitao, H. Nakai, M. Klene, X. Li, J. E. Knox, H. P. Hratchian, J. B. Cross, C. Adamo, J. Jaramillo, R. Gomperts, R. E. Stratmann, O. Yazyev, A. J. Austin, R. Cammi, C. Pomelli, J. W. Ochterski, P. Y. Ayala, K. Morokuma, G. A. Voth, P. Salvador, J. J. Dannenberg, V. G. Zakrzewski, S. Dapprich, A. D. Daniels, M. C. Strain, O. Farkas, D. K. Malick, A. D. Rabuck, K. Raghavachari, J. B. Foresman, J. V. Ortiz, Q. Cui, A. G. Baboul, S. Clifford, J. Cioslowski, B. B. Stefanov, G. Liu A. Liashenko, P. Piskorz, I. Komaromi, R. L. Martin, D. J. Fox, T. Keith, M. A. Al-Laham, C. Y. Peng, A. Nanayakkara, M. Challacombe, P. M. W. Gill, B. Johnson, W. Chen, M. W. Wong, C. Gonzalez and J. A. Pople, Gaussian 03, Revision B.01, Gaussian, Inc., Pittsburgh PA, (2003).
[19] J. Tomasi, B. Mennucci, R. Cammi, Chem. Rev. 105 (2005) 2999.

[20] D.C. Young, Computational chemistry: a practical guide for applying techniques to real-world problems, John Wiley & Sons, Inc., NY, (2001).
[21] N.K. Chaudhary, Archives of Applied Science Research, 5/16 (2013) 227-231.
[22] J.M.W. Scott, W.H. Jura, Can. J. Chem., 45 (1967) 2375.
[23] F.D. Popp, H.P. Schultz, Chem. Rev., 62 (1962) 19.
[24] J.P. Coleman, In: The chemistry of acid derivatives, Suppl. B, Ed. S. Patai, Wiley-Interscience, NY, (1979) 782-824.
[25] J.K. Leland, M.J. Powell, J. Electrochem. Soc., 137 (1990) 3127.
[26] F. Brovelli, B. L. Rivas, J.C. Bernède, J. Chil. Chem. Soc., 50 (2005) 597-602.
[27] C.I. Simionescu, I. Cianga, M. Ivanoiu, Al. Duca, I. Cocarla, M. Grigoras, Eur. Polym. Journ., 35 (1999) 587-599.
[28] O. Hammerich, In: Organic Electrochemistry, H. Lund, O. Hammerich, (Eds.), 4th Ed., Marcel Dekker, NY, (2001) 109.
[29] V. Jouikov, J. Simonet, In: Encyclopedia of Electrochemistry, vol. 8, A. Bard, M. Stratman, H. Shaefer (Eds.), Wiley-VCH, New York, (2004) 235.
[30] C. Hansch, A. Leo, R. W. Taft, Chem. Rev., 97 (1991) 165-195.
[31] A.R. Cherkasov, V.I. Galkin, R.A. Cherkasov, Rus. Chem. Rev., 65 (1996) 695-711.
[32] M. Boulkroune, L. Ignatovich, V. Muravenko, J. Spura, A. Chibani, V. Jouikov, Chem. Heterocycl. Comp., 11 (2013) 1706-1715.
[33] S. Soualmi, L. Ignatovich, E. Lukevics, A. Ourari, V. Jouikov, J. Organomet. Chem., 693 (2008) 1346-1352.
[34] V.F. Sidorkin, E.F. Belogolova, Y. Wang, V. Jouikov, E.P. Doronina, Chem. Eur. J., 8 (2017) 1910-1919.
[35] R.G. Pearson, Chemical Hardness, Wiley-VCH, Weinheim, (1997) 27.
[36] G. Klopman, J. Am. Chem. Soc., 90 (1968) 223.
[37] The Reactivity and Reaction Pathways [Russ. transl.], G. Klopman (Ed.), Mir, Moscow, (1977) 383.
[38] D.L. Nelson, M.M. Cox, Lehninger Principles of Biochemistry, W.H. Freeman and Co., New York, (2005) 157.
[39] H.F. Gilbert, Basic Concepts in Biochemistry, 2nd ed., McGraw-Hill Co., Inc., (2000) 304.
[40] M. Nath, N. Chaudhary, Synth. React. Inorg. Met.-Org. Chem., 28 (1998) 121-133.
[41] H.H. Freedman, J. Am. Chem. Soc., 83 (1961) 2900.
[42] A. Rani, M. Kumar, R. Khare, H. S. Tuli, J. Biol. Chem. Sci., 2/1 (2015) 62–91.
[43] A.M. Abu-Dief, I.M.A. Mohamed, J. Basic and Appl. Sci., 4 (2015) 119–133.
[44] J.-I. Yoshida, T. Maekawa, T. Murata, S.-I. Matsunaga, S. Isoe, J. Am. Chem. Soc. 112 (1990) 1962.

Dalton Transactions

PAPER

View Article Online
View Journal | View Issue

Cite this: *Dalton Trans.*, 2018, **47**, 17127

Halogen-free GeO_2 conversion: electrochemical reduction *vs.* complexation in $(DTBC)_2Ge[Py(CN)_n]$ (n = 0...2) complexes†

Elena N. Nikolaevskaya, [a] Evgeniya A. Saverina,[a,b] Alyona A. Starikova,[c] Amel Farhati,[b] Mikhail A. Kiskin, [d] Mikhail A. Syroeshkin, *[a] Mikhail P. Egorov[a] and Viatcheslav V. Jouikov *[b]

Received 20th August 2018,
Accepted 5th November 2018

DOI: 10.1039/c8dt03397h

rsc.li/dalton

3,5-di-*tert*-Butylcatecholate (DTBC) germanium complexes $(DTBC)_2Ge[Py(CN)_n]_2$ (n = 0...2) have been synthesized from GeO_2, 3,5-di-*tert*-butylcatechol and cyano-substituted pyridines $Py(CN)_n$ and characterized by elemental analysis, NMR, IR and UV-VIS spectroscopy. The structure of **1** (with 4-cyanopyridine) has been determined by X-ray single crystal analysis. UV-VIS spectra have shown that these complexes are stable in CH_3CN, toluene and CH_2Cl_2 solutions; in contrast, they are rapidly decomposed by dimethylformamide and tetrahydrofuran. Complexes **1** and **2** (with 4-cyano and 3-cyanopyridine) are electrochemically reducible in toluene/1 M Bu_4NPF_6 at E = –1.3...–1.7 V *vs.* AgCl. The quantum-chemical study of these complexes is in accordance with the unsuccessful attempts to obtain analogous derivatives with 2-cyanopyridine and 2,6-dicyanopyridine.

Introduction

Although the annual world's consumption of Ge is relatively small (134 tons in 2017[1]), germanium is a strategic element with high ecological value. Besides IR optic fibers and devices,[2] photovoltaics[3] and Si/Ge semiconductor electronics,[4] germanium shows great promise for manufacturing anodic materials for lithium-ion batteries of new generation, the energy efficiency of such materials exceeding that of graphite and tin by more than 4 and 1.6 times, respectively.[5,6] In addition, the electrical conductivity of germanium is 100 times higher and the diffusion efficiency of Li^+ is 400 times greater than that of silicon.[7]

The compound used as a source of Ge for any practical applications is germanium(IV) dioxide. It is chemically inert (0 out of 4 on the scale of NFPA 704) and nontoxic (1/4 NFPA 704, the National Fire Protection Association is the leading information and knowledge resource on fire, electrical and related hazards) with germanium and oxygen atoms forming a polymer network.[8] In order to enable further conversion, the latter must be somehow disassembled; usually it involves the transformation of GeO_2 into $GeCl_4$, which is suitable for nucleophilic displacement reactions[9] or for electroreduction leading to germanium nanoparticles.[10] It is worth noting that these two processes are formally similar: in the electrochemical context, the electron acts as an elementary nucleophile and both processes result in the elimination of Cl^- anions.

In contrast to GeO_2, $GeCl_4$ is highly toxic (3/4 NFPA,) and air-unstable (2/4 NFPA). These facts complicate the processing of the latter compound in the laboratory and in industry. The development of halogen-free methods of metal conversion for modern green chemical technology is therefore of the utmost importance, as was emphasized by the IUPAC.[11]

One of the available alternatives for the development of halogen-free methods of GeO_2 conversion to target products is the reaction with aromatic 1,2-diols (catechols). Discovered in 1954 by P. Bevillard,[12] this reaction is characterized by the simplicity of conditions (water and moderate heating) and the safety of the reagents used: catechols are benign chemical compounds widely present in nature (dihydroquercetin and other natural antioxidants)[13] and in living organisms (epinephrine, related catecholamines, *etc.*).[14]

Using catechols, germanium can be extracted from the GeO_2 polymer matrix to form a soluble molecular compound that can be functionalized or electrochemically reduced on the same principles as in chlorine technology, but without the dis-

[a]*N.D. Zelinsky Institute of Organic Chemistry RAS, Moscow, Russia. E-mail: syroeshkin@ioc.ac.ru*
[b]*UMR CNRS 6226 ISCR, University of Rennes 1, Rennes, France. E-mail: vjouikov@univ-rennes1.fr*
[c]*Institute of Physical and Organic Chemistry at Southern Federal University, Rostov on Don, Russia*
[d]*N.S. Kurnakov Institute of General and Inorganic Chemistry RAS, Moscow, Russia*

†Electronic supplementary information (ESI) available: NMR spectra and computational data. CCDC 1841301. For ESI and crystallographic data in CIF or other electronic format see DOI: 10.1039/c8dt03397h

advantages of the latter. A main problem of the aforementioned approach is that the germanium catechol complex is quite chemically inert. It is the reverse side of its stability and safety. However, germanium in this form can be activated using its propensity for hypercoordination with N-donor ligands. Recently, using pyridine as the N-donor ligand, this halogen-free approach has been successfully realized by the Baines group[15] for the preparation of various organogermanium products. It is worth noting that a wide variety of such hexacoordinated germanium compounds have been obtained recently using 3,5-di-*tert*-butylbenzoquinone-1,2 and metallic germanium in the presence of different N-donor ligands.[16]

On the other hand, complexes of germanium halides with electroreducible N-aromatic ligands were shown to easily accept an electron (at very moderate cathodic potentials) leading to a variety of Ge-centered reactive intermediates (radicals, anions[17]).

With the above said in mind, we thought of introducing an electrochemically reducible ligand into a metal coordination sphere of the germanium–catecholate complex enabling the electrochemical triggering of further nucleophilic reactions. Since pyridine itself is not electroreducible under electrochemical conditions, the most obvious way is choosing a pyridine with an electron-acceptor substituent which would make it electrochemically active;[18] however, the N-donor properties and coordinating ability of such ligands are obviously decreased for electronic reasons. So, a main question is finding an appropriate compromise between these opposite features – stability of the resulting complex and its reducibility. In this contribution, we have explored the possibility of preparing such complexes based on 3,5-di-*tert*-butylcatechol and cyano-substituted pyridines and assessed their suitability for the electrochemical activation in view of developing a halogen-free redox way of germanium conversion. It should be noted that pyridines with acceptor substituents occur in nature (in particular, nicotinic acid and nicotinamide, named vitamin PP).

Results and discussion

3,5-di-*tert*-Butylcatecholate germanium complexes have been synthesized by the reaction of germanium oxide, 3,5-di-*tert*-butylcatechol and different N-donor ligands in a ratio of 1 : 2 : 2 in a toluene/H_2O mixture by the protocol proposed in ref. 15, but without mechanochemical activation of germanium oxide. The reaction mixture was refluxed for 5 hours until total dissolution of GeO_2. In the case of 4-cyano and 3-cyanopyridine, complexes **1** and **2** have been obtained in high yields after the crystallization from toluene (Scheme 1). The known analogous complex with non-substituted pyridine **3**[15] could be easily and efficiently (86% yield) prepared using this technique. At the same time, all attempts to obtain similar germanium complexes **4** and **5** with, respectively, 2-cyanopyridine and 2,6-dicyanopyridine failed. This, at first sight, controversial feature has been elucidated below using quantum chemical calculations.

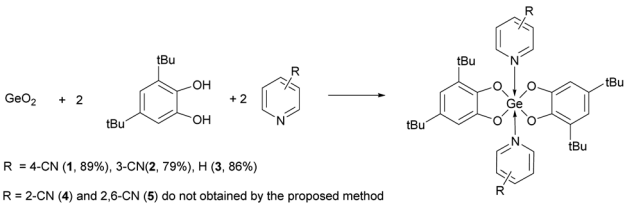

Scheme 1 Synthesis of the complexes **1**, **2** and **3**.

Elemental analysis of all of the obtained products confirmed the stoichiometric structure of $(DTBC)_2GeL_2$ (DTBC = 3,5-di-*tert*-butylcatecholate, L = 4-cyanopyridine and 3-cyanopyridine). These compounds are stable at temperatures up to 160 °C, decomposing without melting above this point.

The obtained complexes have been characterized by IR, and NMR spectroscopy and mass-spectrometry. The IR spectra of **1** and **2** feature distinct medium to strong C–H stretching vibration bands; the O–H vibration modes, typical of 3,5-di-*tert*-butylcatechol, are absent. The latter fact univocally indicates the formation of the corresponding molecular complexes. The NMR spectra of **1** and **2** contain the signals of *tert*-butyl groups and multiple resonances of the aromatic protons of catecholate and pyridine moieties. The proton signals of cyanopyridines in these complexes are shifted upfield compared to the ^{1}H NMR spectra of non-coordinated compounds.[19] The signals shifting in the NMR spectrum of the obtained complexes **1** and **2** in comparison with the initial cyanopyridines indicate the electron density displacement from an organic ligand to a metal atom and the formation of target molecular complexes.

The molecular structure of **1** was confirmed by single crystal X-ray diffractometry. The complex **1** crystalizes in the monoclinic space group $P2_1/c$ as a solvate with one molecule of toluene (**1**·C_7H_8). The Ge atom is situated at the inversion center and has an octahedron environment (Fig. 1). The metal atom is surrounded by two chelating catecholate ligands (Ge(1)–O(1) 1.839(2), and Ge(1)–O(2) 1.841(2) Å) in the equatorial plane and by two N atoms of pyridines (Ge(1)–N(1) 2.136(3) Å)

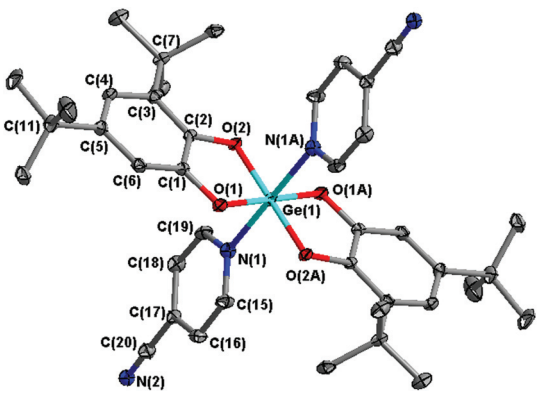

Fig. 1 The ORTEP structure drawing of **1**. Thermal ellipsoids are shown with 50% probability, H atoms are not shown.

at the apical positions. The Ge–O and Ge–N distances in **1** are comparable to those in a similar $(DTBS)_2GePy_2$ complex (Ge–O(1) 1.8471, Ge–O(2) 1.8495 and Ge–N 2.0975 Å (ref. 15)) though Ge–O contacts are a little shorter whereas the Ge–N contact is somewhat longer because of weaker electron donation from cyanopyridine.

The C–O and C–C (in the C6 ring) distances in the 3,5-di-*tert*-butylcatechol ligand in **1** (C–O 1.368(4), 1.372(4) Å and C–C 1.377(4)–1.409(4) Å) are typical of catecholate bond lengths (C–O 1.35–1.38 Å and C–C 1.41–1.45 Å).[20] The two catechol aromatic units face two Py ligands to form a water wheel resembling structure.

Complexes **1** and **2** are very poorly soluble in saturated hydrocarbons such as pentane or hexane but have a fair solubility in non-coordinating or weakly-coordinating toluene, CH_2Cl_2, $CHCl_3$ and MeCN. Although parent cyano-substituted pyridines and germanium catecholate complexes are colorless, **1** and **2** were isolated as orange and yellow solids correspondingly. Their UV-vis spectra in toluene solution are shown in Fig. 2. The color of **1** (a pronounced absorption maximum at λ_m = 406 nm) probably corresponds to a charge-transfer band. According to the TD-DFT calculation results (Fig. S1†), absorption in the region of 400 nm in compound **1** corresponds to a charge-transfer band from the catecholate ligand to pyridine (ligand-to-ligand charge transfer – LLCT). Complex **2** also absorbs in the visible region, at shorter wavelengths, but it does not have a distinct maximum.

The non-substituted pyridine forms the strongest complex **3** that is colorless both as a solid and in solution. UV-VIS spectra of **1–2** in the solid state are identical to those shown in toluene solution.

It should be noted that complexes **1** and **2** show a rapid decay of their characteristic absorption when THF or DMF is added to their toluene solutions (Scheme 2). Upon the addition of even 10 vol% of THF to the toluene solution of **1**, its color is substantially attenuated after several minutes (Fig. 3). This can be rationalized by the better coordinating ability of THF compared to MeCN, CH_2Cl_2 or toluene (the corresponding donor numbers, DN, of these solvents are 20.0, 14.1, 1 and 0.1, respectively[21]). Bis-catecholate complexes

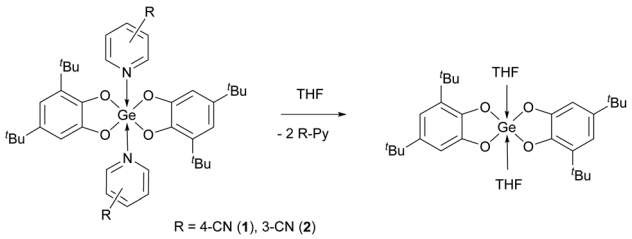

Scheme 2 THF/cyanopyridine ligand exchange in complexes **1** and **2**.

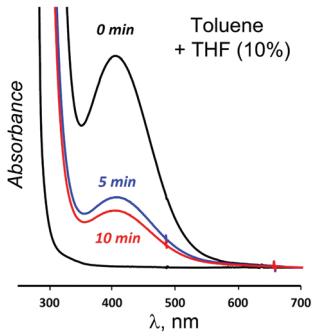

Fig. 3 UV-Vis spectra of **1** (1 mmol L^{-1} in $PhCH_3$) before and after addition of 10% (vol) of THF.

of germanium with THF (DN = 20) and other ethers are also known [20i]; apparently DMF and THF are more efficient ligands and can substitute cyanopyridines in the coordination sphere of Ge so that the resulting species are devoid of the target redox properties sought for.

As we expected, complexes **1** and **2** are electrochemically reducible in CH_2Cl_2/0.1 M Bu_4NBF_4 (at T = 293 K) or in toluene/1 M Bu_4NBF_4 (T = 313 K); in the second system their reduction signals are better shaped because of better ohmic drop compensation. The reduction of **1** even shows a partial reversibility of electron transfer (ET) at ν 0.1 V s^{-1}, which is supposedly related to the reversibility of reduction of the parent 4-cyanopyridine (Fig. 4). The reduction potentials of

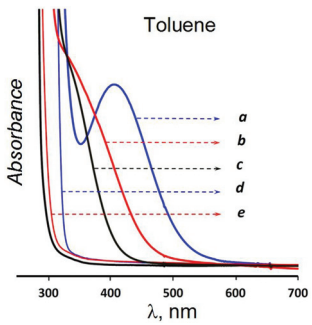

Fig. 2 UV-Vis spectra of 1 mmol L^{-1} solutions in toluene: (a) **1**, (b) **2**, (c) **3**, (d) non-coordinated 3-cyanopyridine and (e) 4-cyanopyridine. T = 293 K.

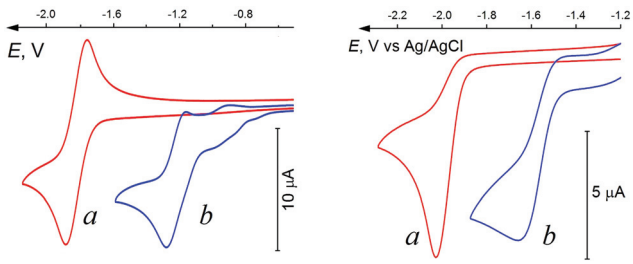

Fig. 4 Cyclic voltammetry in toluene/1 M Bu_4NBF_4 at a GC working electrode. Left: Reduction of (a) 4-cyanopyridine (4 mmol L^{-1}) and (b) **1** (2 mmol L^{-1}). Right: (a) 3-Cyanopyridine (4 mmol L^{-1}) and (b) **2** (2 mmol L^{-1}). Scan rate v = 0.1 V s^{-1}, T = 313 K.

these complexes E_p (−1.275 V and −1.670 V *vs.* Ag/AgCl for **1** and **2**, respectively) are substantially shifted to the positive potentials compared to the E_ps of the parent cyanopyridines (Fig. 4).[22] Most to our surprise, **3** has also shown a reduction step with the potential falling in between E_p(**1**) and E_p(**2**), E_p(**3**) = −1.590 V. This is quite unexpected because the reduction of these complexes is supposed to affect the nitrogen ligand while pyridine itself is not reducible under these conditions (*i.e.* E_p(Py) < −2.9...−3 V). The large shifts in E_ps of **1** and **2** (+630 mV gain in E_p for **1**, +375 mV for **2**, and more than +1400 mV for **3**) reflect dative electron delocalization from these ligands to Ge, the Lewis acid center of the $(DTBS)_2Ge$ catecholate complex, facilitating ET to the pyridine units and thus opening the gate for the incoming electron to the whole $(DTBC)_2Ge[Py(CN)]_2$ system. This effect, resembling the introduction of electron-withdrawing substituents to the Py units, is akin to the facilitation of the electroreduction of the complexes of halosilanes and halogermanes with 2,2′-bipyridine.[17] Repeating the scans led to the passivation of the electrode, supposedly by the deposition of elemental Ge (*cf.* the formation of Ge from the reduction of similar complexes with $LiAlH_4$ [15]).

In order to reveal the factors responsible for the propensity of germanium(IV) bis-catecholate complexes to reduction and to locate the sites of the electron uptake, the DFT orbital analysis of $(DTBC)_2Ge$ and of its pyridine complexes **1**, **2** and **3** has been performed using a B3LYP/def2tzvp protocol. It is a suitable protocol for 14 group metal complexes.[23]

It is well seen (Fig. 5) that in $(DTBC)_2Ge$ the LUMO and SOMO are mostly localized on the Ge atom while in its N-base complexed derivatives **1**–**3** the sites of ET are different. In $(DTBC)_2Ge$, an incoming electron will directly affect the electrophilic Ge (the DTBC ligands, initially not participating in the LUMO, accommodate some electron density by back bonding from Ge in the radical anion, Fig. 5b). In **1**, **2** and **3**, the LUMO is doubly degenerated being located on two equivalent ligands (Fig. 5c); ET will thus populate the π*-system of the pyridine ligands removing the degeneracy in the anion radical.

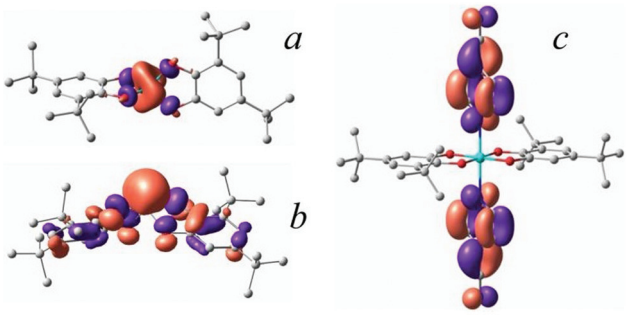

Fig. 5 (a) LUMO of the $(DTBC)_2Ge$ complex and (b) its SOMO after one-electron uptake. (c) Ligand-localized doubly degenerate LUMO of **1**. From DFT B3LYP/def2tzvp calculations (cutoff = 0.04). Hydrogen atoms are omitted for clarity.

Considering the relative enthalpies of the formation of the complexes ΔH_f from DFT B3LYP/def2tzvp (with the SMD model of nonspecific solvation in toluene) frequency analysis, one can see that they correlate well with the easiness of the reduction of the complexes and their stability (Fig. 6). Indeed, both ΔH_f and $\Delta E_p^{(Py-ligand)-(Complex)}$ follow the same order: **3** > **1** > **2** (the larger ΔH_f, the more E_p is shifted compared to the E_p of the parent pyridine ligand, *vide supra*). On the other hand, thermochemistry of the formation of **1**–**5** (for fully optimized structures, Fig. 6 and Table S1†) allows one to rationalize the unsuccessful attempts to isolate **4** and **5**. As follows from the computational data, the formation of **1**, **2**, and **3** from $(DTBC)_2Ge$ and two pyridine derivatives (Table S1†) is thermodynamically favored by more than −18 kcal mol^{-1}. This parameter for **4** is more than twice smaller, ΔH_f = −6.8 kcal mol^{-1} only, which seems to be insufficient to allow the isolation of this complex. Despite the fact that theoretically **4** could exist, only a mixture of the bis-catecholate germanium complex without any ligands and the initial non-coordinated 2-cyanopyridine is observed according to NMR spectroscopy.

The computational structural parameters of **4** also reveal the substantial elongation of the coordination bonds Ge–N (2.257 Å against 2.17–2.19 Å in isolated complexes **1**–**3**). The repulsion of the cyano group with two p_z-type *n* electrons of oxygen atoms entails a remarkable deviation of the cyano group from linearity (the bent angle of the C–C–N unit is 171.6°) as well as lengthening and weakening the Ge–N coordination contact. Further enhancement of this feature in **5** containing two 2,6-dicyanosubstituted pyridine units (the Ge–N bonds are stretched to 2.424 Å and the ∠C–C–N angle progressed to 168.9°) leads to the positive formation enthalpy, ΔH_f = 13.5 kcal mol^{-1}, precluding the formation of this complex. The steric reason seems to dominate over the electronic one because **2** with the CN group in the *meta*-position is isolable, while **4**, with a less conjugated (hence less destabilizing) but exerting stronger steric hindrance CN group, is not.

Experimental

GeO_2 was purchased from "Germanium and Applications Ltd" (DG-B, TY 1774-001-95961127-2010, batch #117); 3,5-di-*tert*-butylcatechol, 4-cyanopyridine and 3-cyanopyridine (Aldrich) were used without further purification. Solvents were purified by standard methods.[24] All manipulations were carried out under an argon atmosphere.

^{1}H NMR (300 MHz) and ^{13}C NMR (75 and 125 MHz) spectra were recorded on Bruker AM300 and Bruker DRX500 spectrometers in $CDCl_3$ at ambient temperature using tetramethylsilane as an internal standard. FTIR spectra of complexes were recorded on a BRUKER Vertex-70 FTIR spectrometer. Elemental analysis was performed using an elemental Vario EL spectrophotometer.

UV-Vis spectra were recorded with an Agilent 8453 instrument using a 10 mm quartz cell. Cyclic voltammetry was

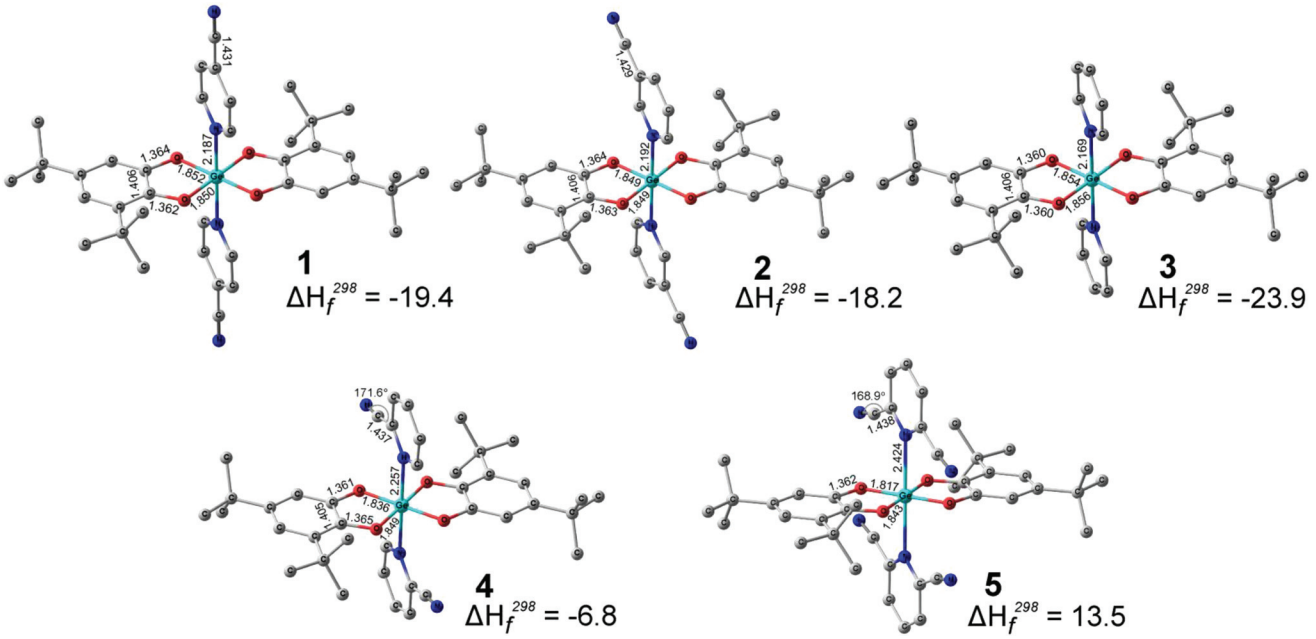

Fig. 6 Optimized geometries (bond lengths per Å, angles per degrees) and formation enthalpies taking into account the nonspecific solvation (SMD, solvent–toluene) (kcal mol^{-1}) of 3,5-di-*tert*-butylcatecholate germanium complexes with pyridines from DFT B3LYP/def2tzvp calculations. Hydrogen atoms are omitted for clarity.

carried out using a PC-piloted digital potentiostat IPC-Pro-MF (Econix). A standard thermostated (T = 25 ± 0.5 °C) 10 ml electrochemical cell was used in a three-electrode configuration. As a working electrode, a GC (1.7 mm) disk was used, polished before each run; a Pt wire was used as an auxiliary electrode. The potentials are referred to the AgCl/KCl sat. electrode separated from the analyte by an electrolytic bridge filled with the same solution. All measurements were carried out under dry argon.

Density functional theory (DFT) calculations were performed using the Gaussian 09 program package[25] at the B3LYP/def2tzvp level. It has been recently shown[26] that the B3LYP functional gives accurate reproduction of the geometry, energy and other characteristics (in particular, coordination of base molecules) of main-group element bis-chelate complexes with redox-active ligands; def2tzvp is currently one of the highest level basis sets used when optimizing the geometry of coordination compounds containing 100 or more atoms. The stationary points on the potential energy surfaces were located by full geometry optimization with the calculation of the force constant matrix and checked for the stabilities of the DFT wave function. Structural visualizations in Fig. 5 and 6 were produced with the program suite ChemCraft.[26]

Single crystals of **1** for X-ray data collection were taken from the reaction mixtures and stored under matrix liquors. The X-ray data were collected on a Bruker APEX II diffractometer equipped with a CCD camera and a graphite-monochromated Mo-K$_\alpha$ radiation source (λ = 0.71073 Å).[27] The structure was solved by direct methods and using Fourier techniques and were refined by full-matrix least squares against F^2 with anisotropic displacement parameters for all non-hydrogen atoms. Positions of disordered Me-groups in the *tert*-butyl fragment (at the C(11) atom) of 3,5-^{t}BuCat were localized in difference Fourier maps and refined with occupancies of 0.296(6) and 0.704(6). Positions of disordered solvate molecules of toluene were localized in difference Fourier maps and refined with occupancies of 0.374(9) and 0.626(9). Refinement of the disordered Me-groups in the *tert*-butyl fragment and toluene molecule was done with restrains (DFIX and RIGU for both, FLAT for toluene). The hydrogen atoms bound to carbon were positioned geometrically and refined using the riding model. All calculations were carried out with the use of the SHELX2014/6 software package.[28] The crystallographic parameters for **1** at T = 150(2) K were as follows: $C_{54}H_{64}GeN_4O_4$, fw = 905.68, yellow, parallelepiped, crystal size 0.12 × 0.08 × 0.06, monoclinic system, space group $P2_1/c$, a = 15.082(2) Å, b = 22.183(2) Å, c = 7.3630(8) Å, β = 94.243(2)°, V = 2456.7(4) Å^3, Z = 2, ρ_{calc} = 1.224 g cm^{-3}, μ = 0.672 cm^{-1}, 20 699 measured reflections, 3520 reflections with $I > 2.0\sigma(I)$, R_{int} = 0.104, GooF = 1.01, R_1 ($I > 2\sigma(I)$) = 0.051, wR_2 ($I > 2\sigma(I)$) = 0.125, R_1 (all data) = 0.101, wR_2 (all data) = 0.161. CCDC 1841301† contains the supplementary crystallographic data for **1**.

General procedure for the synthesis of 1 and 2

Complex 1. To a suspension of GeO_2 (0.071 g, 0.7 mmol) in water (15 ml), 3,5-di-*tert*-butylcatechol (0.3 g, 1.3 mmol) and 4-cyanopyridine (0.141 g, 1.3 mmol) in toluene (15 ml) were added. The reaction mixture was refluxed for 5 hours until the total disappearance of GeO_2. Then the solvents were removed using a rotary evaporator and the crude product has been

recrystallized from toluene to give an orange powder (0.45 g, 89%).

^{1}H NMR (300 MHz, $CDCl_3$, δ, ppm): 1.20 and 1.41 (both s, 9H, *t*Bu), 6.57 and 6.79 (both s, 1H, H_{tBuCat}), 7.66 and 9.14 (both d, 2H, H_{Py}, J = 4.98 Hz). ^{13}C NMR (75 MHz, $CDCl_3$, δ, ppm): 29.80 ($(\underline{C}H_3)_3C$), 31.66 ($(\underline{C}H_3)_3C$), 34.34 ($(CH_3)_3\underline{C}$), 34.69 ($(CH_3)_3\underline{C}$), 148.11 (C_{Py}), 126.88 (C_{Py}), 124.12 (C_{Py}), 115.00 (C_{Py}), 108.56 (C_{Cat}), 112.93 (C_{Cat}), 129.02 (C_{Cat}), 133.46 (C_{Cat}), 140.29 (C_{Cat}), 142.20 (C_{Cat}). FTIR (KBr, cm^{-1}): 3128w, 3108w, 3077w, 2962m, 1654w, 1616m, 1577m, 1477m, 1445w, 1418s, 1361m, 1318m, 1284m, 1237s, 1210m, 1025s, 982s, 858m, 848s, 828w, 809m, 757m, 733w, 719w, 675w, 564s, 505w, 459w. MS (EI, 70 eV): molecular ion M^+ is unstable, m/z 514 corresponds to the ion after the loss of N-donor ligands. Anal. Calcd for $C_{40}H_{48}GeN_4O_4$: C, 66.59; H, 6.71; Ge, 10.07; N, 7.77. Found: C, 66.89; H, 6.56; Ge, 10.34; N, 7.61.

Complex 2. Prepared as described for **1** from GeO_2 (0.09 g, 0.86 mmol), 3,5-di-*tert*-butylcatechol (0.38 g, 1.7 mmol) and 3-cyanopyridine (0.178 g, 1.7 mmol). Complex **2** was isolated from toluene as yellow powder (0.40 g, 79%).

^{1}H NMR (500 MHz, $CDCl_3$, δ, ppm): 1.21 and 1.44 (both s, 9H, *t*Bu), 6.59 and 6.82 (both d, 1H, H_{tBuCat}, J = 1.33 Hz), 7.58 (m, 1H, H_{Py}), 8.07 (m, 1H, H_{Py}), 9.14 (m, 1H, H_{Py}), 9.25 (m, 1H, H_{Py}). ^{13}C NMR (125 MHz, $CDCl_3$, δ, ppm): 30.22 ($(\underline{C}H_3)_3C$), 32.10 ($(\underline{C}H_3)_3C$), 34.8 ($(CH_3)_3\underline{C}$), 35.1 ($(CH_3)_3\underline{C}$), 109.14, 113.36, 125.63, 134.01, 140.91, 142.53, 146.78, 150.83. FTIR (KBr, cm^{-1}): 2956s, 2868w, 1605m, 1574w, 1474s, 1441m, 1418s, 1363w, 1328m, 1283m, 1263w, 1223s, 1210w, 1185m, 1063w, 1028w, 985s, 917w, 855m, 831m, 811s, 758s, 722w, 689m, 656m, 555w, 461m. MS (EI, 70 eV): m/z 514 ($M^+ - 2$ PyCN). Anal. Calcd for $C_{40}H_{48}GeN_4O_4$: C, 66.59; H, 6.71; Ge, 10.07; N, 7.77. Found: C, 66.73; H, 6.46; Ge, 10.15; N, 7.59.

Conclusions

The introduction of a pyridine ligand into non-reducible bis-catecholate germanium derivatives permits the activation of such complexes and involves them in electron uptake reactions. This is underpinned by a fine interplay between two opposite phenomena: the coordinating (donating) ability of pyridine ligands and the ease (electron affinity) of their own reduction. Compared to $GeCl_4$, the electrophilicity of Ge in the $(DTBC)_2Ge$ complex and therefore its proneness to reduction are strongly hampered to the point that it is not reducible within the cathodic range of potentials in conventional solvents; the coordination with a nitrogen base only enhances this feature. However, the electron-deficient π^*-system of pyridines opens up the way to inject an extra electron to the $(DTBC)_2Ge[Py(CN)]_2$ system and to trigger its nucleophilic reactivity. In the first place, it might be useful for preparing/recycling elemental Ge in a halogen-free process and other applications. Note that cyano-pyridines, just as many catechols, are non-toxic and they are widespread in nature as compounds with pronounced beneficial biological properties. Further studies in this field are under progress.

Conflicts of interest

There are no conflicts to declare.

Acknowledgements

The work was supported by the Russian Science Foundation (grant no. 17-73-20281). Single crystal X-ray diffraction analysis was performed at the User Facilities Centers of IGIC RAS. M. A. K. thanks the Russian Academy of Science for the financial support of X-ray diffraction studies.

Notes and references

1 C. L. Thomas, *Germanium, 2018 Minerals Yearbook*, USGS Publications, 2018, https://minerals.usgs.gov/minerals/pubs/commodity/germanium/mcs-2018-germa.pdf, accessed 28.07.2018.
2 M. Ordu, J. Guo, G. Ng Pack, P. Shah, S. Ramachandran, M. K. Hong, L. D. Ziegler, S. N. Basu and S. Erramilli, *AIP Adv.*, 2017, **7**, 095125, DOI: 10.1063/1.5003027.
3 M. Zurch, H.-T. Chang, L. J. Borja, P. M. Kraus, S. K. Cushing, A. Gandman, C. J. Kaplan, M. H. Oh, J. S. Prell, D. Prendergast, C. D. Pemmaraju, D. M. Neumark and S. R. Leone, *Nat. Commun.*, 2017, **8**, 15734, DOI: 10.1038/ncomms15734.
4 B. Bonham and G. Guisbiers, *Nanotechnology*, 2017, **28**, 245702, DOI: 10.1088/1361-6528/aa726b.
5 C. Yang, Y. Jiang, X. Liu, X. Zhonga and Y. Yu, *J. Mater. Chem. A*, 2016, **4**, 18711–18716, DOI: 10.1039/C6TA08681K.
6 J. Wu, Z. Zhu, H. Zhang, H. Fu, H. Li, A. Wang and H. Zhang, *Sci. Rep.*, 2016, **6**, 29356, DOI: 10.1038/srep29356.
7 X. Xiao, X. Li, S. Zheng, J. Shao, H. Xue and H. Pang, *Adv. Mater. Interfaces*, 2017, 1600798, DOI: 10.1002/admi.201600798.
8 J. W. E. Drewitt, P. S. Salmon, A. C. Barnes, S. Klotz, H. E. Fischer and W. A. Crichton, *Phys. Rev. B: Condens. Matter Mater. Phys.*, 2010, **81**, 014202, DOI: 10.1103/PhysRevB.81.014202.
9 *Science of synthesis: Houben-Weyl methods of molecular transformations, Category 1: Organometallics, Vol. 5: Compounds of group 14 (Ge, Sn, Pb)*, ed. M. Maloney, Georg ThiemeVerlag, Stuttgart, New York, 2003.
10 K. Nadarajah, A. F. Khan and N. A. Rahim, *Recent Pat. Nanotechnol.*, 2016, **10**, 26, DOI: 10.2174/2210315506999160304132606.
11 P. Tundo, *Pure Appl. Chem.*, 2012, **84**, vi.
12 P. Bevillard, *Bull. Soc. Chim. Fr.*, 1954, 296.
13 Y. Chen and P. Deuster, *Chem.-Biol. Interact.*, 2009, **182**, 7, DOI: 10.1016/j.cbi.2009.06.007.
14 G. Eisenhofer, I. J. Kopin and D. S. Goldstein, *Pharma Rev.*, 2004, **56**, 331, DOI: 10.1124/pr.56.3.1.

15 M. Glavinovic, M. Krause, L. Yang, J. A. McLeod, L. Liu, K. M. Baines, T. Friscic and J.-P. Lumb, *Sci. Adv.*, 2017, **3**, e1700149, DOI: 10.1126/sciadv.1700149.

16 (*a*) A. A. El-Hadad, B. R. McGarvey, B. Merzougui, R. G. W. Sung, A. K. Trikha and D. G. Tuck, *J. Chem. Soc., Dalton Trans.*, 2001, **7**, 1046–1052; (*b*) N. Konopic, G. Liptay, H. Blana and S. Bachmayer, *J. Therm. Anal.*, 1974, **6**, 231–235.

17 (*a*) M. Dieng, D. Gningue-Sall and V. V. Jouikov, *Main Group Met. Chem.*, 2012, **35**, 141, DOI: 10.1515/mgmc-2012-0059; (*b*) S. Soualmi, M. Dieng, A. Ourari, D. Gningue-Sall and V. Jouikov, *Electrochim. Acta*, 2015, **58**, 457–469, DOI: 10.1016/j.electacta.2015.01.182.

18 J. Eriksen, H. Lund and A. I. Nyvad, *Acta Chem. Scand.*, 1983, **37b**, 459–466, DOI: 10.3891/acta.chem.scand.37b-0459;.

19 AIST, Integrated Spectral Database System of Organic Compounds (National Institute of Advanced Industrial Science and Technology (Japan) // https://sdbs.db.aist.go.jp; accessed 28.07.2018.

20 (*a*) V. K. Cherkasov, G. A. Abakumov, E. V. Grunova, A. I. Poddelsky, G. K. Fukin, E. V. Baranov, Y. V. Kurskii and L. G. Abakumova, *Chem. – Eur. J.*, 2006, **12**, 3916–3927; (*b*) V. K. Cherkasov, E. V. Grunova, A. I. Poddelsky, G. K. Fukin, Yu. A. Kurskii, L. G. Abakumova and G. A. Abakumov, *J. Organomet. Chem.*, 2005, **690**, 1273–1281; (*c*) G. K. Fukin, L. N. Zakharov, G. A. Domrachev, A. U. Fedorov, S. N. Zaburdyaeva and V. A. Dodonov, *Russ. Chem. Bull.*, 1999, **9**, 1744–1753; (*d*) M. Hall and D. B. Sowerby, *J. Am. Chem. Soc.*, 1980, **102**, 628–632; (*e*) R. R. Holmes, R. O. Day, V. Chandrasekhar and J. M. Holmes, *Inorg. Chem.*, 1987, **26**, 157–163; (*f*) R. R. Holmes, R. O. Day, V. Chandrasekhar and J. M. Holmes, *Inorg. Chem.*, 1987, **26**, 163–168; (*g*) Z. Tian and D. G. Tuck, *J. Chem. Soc., Dalton Trans.*, 1993, 1381–1385; (*h*) M. N. Gibbons, M. J. Begley, A. J. Blake and D. B. Sowerby, *J. Chem. Soc., Dalton Trans.*, 1997, 2419–2425; (*i*) A. V. Lado, A. V. Piskunov, I. V. Zhdanovich, G. K. Fukin and E. V. Baranov, *Russ. J. Coord. Chem.*, 2008, **34**, 251–255; H.-C. Chiang, S.-F. Hwang and C.-H. Ueng, *Acta Crystallogr., Sect. C: Cryst. Struct. Commun.*, 1996, **52**, 31–33.

21 L. Malavolta, E. F. Poletti, E. H. Silva, S. Schreier and C. R. Nakaie, *Int. J. Mol. Sci.*, 2008, **9**, 1321, DOI: 10.3990/ijms9071321.

22 J. Volke and V. Skala, *J. Electroanal. Chem.*, 1972, **36**, 383–388, DOI: 10.1016/S0022-0728(72)80260-2.

23 V. Ya. Lee, *Organosilicon compounds. Theory and experiment (synthesis)*, Elsevier, Academic Press, London, 2017.

24 D. D. Perrin, W. L. F. Armarego and D. R. Perrin, *Purification of Laboratory Chemicals*, Pergamon Press, Oxford, 1980.

25 M. J. Frisch, G. W. Trucks, H. B. Schlegel, G. E. Scuseria, M. A. Robb, J. R. Cheeseman, G. Scalmani, V. Barone, B. Mennucci, G. A. Petersson, H. Nakatsuji, M. Caricato, X. Li, H. P. Hratchian, A. F. Izmaylov, J. Bloino, G. Zheng, J. L. Sonnenberg, M. Hada, M. Ehara, K. Toyota, R. Fukuda, J. Hasegawa, M. Ishida, T. Nakajima, Y. Honda, O. Kitao, H. Nakai, T. Vreven, J. A. Montgomery, Jr., J. E. Peralta, F. Ogliaro, M. Bearpark, J. J. Heyd, E. Brothers, K. N. Kudin, V. N. Staroverov, T. Keith, R. Kobayashi, J. Normand, K. Raghavachari, A. Rendell, J. C. Burant, S. S. Iyengar, J. Tomasi, M. Cossi, N. Rega, J. M. Millam, M. Klene, J. E. Knox, J. B. Cross, V. Bakken, C. Adamo, J. Jaramillo, R. Gomperts, R. E. Stratmann, O. Yazyev, A. J. Austin, R. Cammi, C. Pomelli, J. W. Ochterski, R. L. Martin, K. Morokuma, V. G. Zakrzewski, G. A. Voth, P. Salvador, J. J. Dannenberg, S. Dapprich, A. D. Daniels, O. Farkas, J. B. Foresman, J. V. Ortiz, J. Cioslowski and D. J. Fox, *Gaussian 09 (Revision E.01)*, Gaussian, Inc., Wallingford CT, 2013.

26 Chemcraft, http://www.chemcraftprog.com; accessed 28.07.2018.

27 *SMART (Control) and SAINT (Integration) Software, Version 5.0*, Bruker AXS Inc., Madison, WI, 1997.

28 M. Sheldrik, *Acta Crystallogr., Sect. A: Found. Crystallogr.*, 2008, **64**, 112.

Available online at www.joac.info

ISSN: 2278-1862

Journal of Applicable Chemistry

2014, 3 (1): 254-266

(International Peer Reviewed Journal)

Er-YAG/Er-YAP/TiO_2 Composite As A Novel Photocatalyst Using Solar Lights For Treating Aqueous Dye Solutions

Mohamed Faouzi Nsib[1,2] *, Amel Farhati[1], Asma Mayoufi [1], Noomen Moussa [2], Ali Rayes [2] and Ammar Houas[1]

1. URCMEP (UR11ES85), Faculty of Sciences, University of Gabès, 6029 Gabès, **TUNISIA**
2. National School of Engineers (ENIG), University of Gabès, 6029 Gabès, **TUNISIA**

Email: Mohamed.faouzi.ncib@gmail.com

Accepted on 27th December 2013

ABSTRACT

A new photocatalyst for the treatment of aqueous dye solutions under visible and solar lights was designed and prepared. It is based on TiO_2 coating a combination of both upconversion luminescence agents: Er:$Y_3Al_5O_{12}$ (Er-YAG) and Er:$YAlO_3$ (Er-YAP), well known by their ability to transform visible light into UV light. TiO_2 and Er-YAG/Er-YAP/TiO_2 composites were characterized by X-ray diffraction (XRD) and Transmission electron microscopy (TEM). The degradation reaction of methylene blue (MB) aqueous solution was used to measure the photocatalytic activity of the prepared photocatalysts. The obtained results showed that (1.5 % $Er_{0.01}$-YAG + 0.5 % $Er_{0.01}$–YAP)/TiO_2 composite is strongly more photoactive than pure TiO_2 and was able to degrade 98 % of MB solution in one hour under sunlight irradiation at pH = 6.5. This efficiency was supported by TOC measurements and was proven to depend on the ionic nature of the dye and the pH of the solution. Consequently, it is a promising photocatalyst for treating aqueous dye solutions by sunlight.

Keywords: Composite materials, Oxides, Upconversion, Photocatalysis, Wastewater.

INTRODUCTION

The removal of dyes and other commercial stains from the industrial wastewaters is a much concern topic of the environmental safety. During last years, Advanced Oxidation Processes (AOPs) such as UV/H_2O_2, ozonation, (photo) Fenton, sonolysis, electrochemical oxidation, and photocatalysis have been widely and extensively explored to mitigate a great variety of pollutants present in various environmental media. AOPs have been considered as alternatives to conventional water treatment technologies. Among many AOPs, photocatalysis has received huge attention as one of the most viable environmental cleanup technologies [1, 2]. Among a great number of photocatalysts, titanium dioxide (TiO_2) has been used extensively [3, 4]. Its use as photocatalyst is due to some properties such as versatility, physical and chemical stability, abundance, non-toxic as well as a relative low price. However, it is generally accepted that TiO_2 is a poor absorber of photons in the visible spectrum and, as a result, its use as an effective photocatalyst demand a UV light source. From a practical point of view, photocatalysts need to have higher activities to be economically competitive as a cleanup technology. One of the most viable and

practical approaches in developing better photocatalysts is to modify TiO_2 (e.g., impurity doping, sensitization, surface modification/complexation, integration with other nanostructured materials, etc.).For a long time, an immense effort has been provided to extend the absorption wavelength region of TiO_2, i.e., making it absorbing the visible lights significantly. Thus, a lot of solutions have been adopted, such as the doping of transition metal ions or/and the non metals and the combination of semiconductors of narrow band gaps [5-8]. These methods allow extending the absorption range of TiO_2 appreciably, but they often endure a thermal instability and an increase of recombination centers [9]. Some researchers [10] found out that TiO_2 doped with nitrogen (N) absorbs efficiently the visible light without a high increase in its photocatalytic activity. The main reason is that the N-TiO_2 photocatalyst undergoes again a raise of the electron-hole recombination.Besides, the visible light is not so energetic, compared to UV light, to activate the particles of TiO_2 and degrade many organic pollutants efficiently. Therefore, it could be very useful to think about a method of transformation of visible light into UV light that would be more efficient in the activation of TiO_2 particles. Thus, it would be very important to find materials that could transform the visible lights into UV lights to satisfy the real need of the TiO_2 photocatalyst.

Fortunately, the materials of the "upconversion" containing rare earth (RE) metals [11] are just what we want to insert into powders of TiO_2. Most of research studying the upconversion of light has been achieved by physicists looking for materials that produce Laser of short lengths of the wave. The most studied crystals were $LiYF_4$, KYF_4, $Y_3Al_5O_{12}$ (YAG) and $YAlO_3$ (YAP) doped with Er^{3+} ion [12, 13]. Among all the trivalent RE ions, Er^{3+} ion has the richest spectra in the IR-UV range that makes it more adequate for upconversion studies, especially when it is organized in the crystalline matrices of oxides or fluorides [14-17]. The upconversion process depends on the excitation energy, the concentration of doping and the properties of the host crystal.

Lately, these materials have found some interest in photocatalysis, because they may be used to exploit efficiently the inexhaustible solar light in the photodegradation of organic pollutants. Indeed, few studies have especially concerned with upconversion luminescence agents of Er-YAG and Er-YAP type introduced into powders of TiO_2 or ZnO [18, 19]. Photoluminescence measurements have shown that Er-YAG and Er-YAP give out UV lights under excitation in the visible wavelength range [20-22]. Emission spectra are discontinuous and contain distinct peaks for the two types of upconversion agents. Therefore, these spectra do not totally cover the UV domain. As a result, the intensity of UV lights emitted from each upconversion luminescence agent is lower than that of the UV halogen lamp. But if we think to add the emission spectrum of both Er-YAG and Er-YAP, the resultant spectrum of the upconversion process should contain many more peaks, leading to an intensification of UV lights exciting the TiO_2 semi-conductor. Hence, the idea of this study is to exploit simultaneously the most of the upconversion emission spectrum of both Er-YAG and Er-YAP. The procedure consists in coating them together by the TiO_2 powders. This system could improve the kinetics and the yield of the organic pollutants photodegradation. In addition, this system is environmentally feasible since it is based on non-toxic sol-gel synthesized components. Moreover, this system is mainly based on relatively low cost TiO_2 powders, and the expensive upconversion oxides are incorporated only in weak proportions (less than 2 %). This system could also be economically reasonable with regards to the improvement that would be realized in the efficiency of the wastewater remediation processes. In this study, methylene blue (MB: methyl thioninium chloride) was chosen as a probe compound and pollutant for the photocatalytic tests. It is a heterocyclic aromatic compound of positive charge and is usually used as representative for dyes commonly discharged in wastewater.

The photocatalytic activity of prepared $Er_{0.01}$-YAG/$Er_{0.01}$-YAP/TiO_2 composite was studied under visible and solar light irradiation. The molecular structure of MB dye is given in scheme 1.

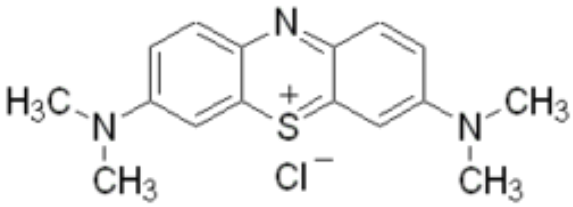

Scheme 1: Molecular structure of methylene blue dye.

MATERIALS AND METHODS

Synthesis of $Er_{0.01}Y_{2.99}Al_5O_{12}$: The nanocrystalline Er-YAG was prepared by a salt based sol-gel process [23]. All chemicals were reactive grade and supplied by Aldrich Inc. Yttrium chloride ($YCl_3.6H_2O$) was dissolved in 100 ml of distilled water, previously mixed with 2 ml of acetic acid (CH_3CO_2H), and the mixture was stirred for 2 h at 50 °C. In a second beaker, proper amounts of aluminum chloride ($AlCl_3.6H_2O$) and erbium nitrate (Er $(NO_3)_3.5H_2O$) were dissolved in 50 ml of distilled water under stirring for 1 h at room temperature. Then both solutions were mixed and complexed with 2 ml of ethylene glycol and stirred again. The resulting solution was stirred at 80 °C for 24 h to evaporate slowly all the solvents until a pale yellow, viscous gel was formed. The gel was dried at 120 °C for 24 h and then ground in an agate mortar to get a fine powder. This powder was annealed at 900 °C for 2 h (ramp 10 °C.min^{-1}). After cooling in air atmosphere, the nanocrystalline $Er_{0.01}Y_{2.99}Al_5O_{12}$ ($Er_{0.01}$-YAG) was obtained.

Synthesis of $Er_{0.01}Y_{0.99}AlO_3$: The nanocrystalline Er-YAP was prepared by the modified nitrate-citric acid method described elsewhere [24]. Briefly, proper amounts of yttrium chloride ($YCl_3.6H_2O$) and erbium nitrate (Er $(NO_3)_3.5H_2O$) were dissolved in 100 ml of distilled water. In a separate flask, aluminum chloride ($AlCl_3.6H_2O$) was dissolved in 50 ml of distilled water and stirred for 1 h at room temperature. Both solutions were mixed and solid citric acid was added (mol. ratio of citric acid: metal ion = 3:1). The final solution was further evaporated at 85 °C until a viscous gel was obtained. The obtained gel was dried at 130 °C for 24 h and ground to get a powder. A heat-treatment of 1200 °C for 2 h (ramp 10 °C.min^{-1}) was applied to the sample. After cooling in air atmosphere, the nanocrystalline $Er_{0.01}Y_{0.99}AlO_3$ ($Er_{0.01}$-YAP) was obtained.

Preparation of TiO_2 photocatalyst coating upconversion luminescence agents: The TiO_2 photocatalyst coating $Er_{0.01}$-YAG and/or $Er_{0.01}$-YAP upconversion luminescence agents was prepared through the soil-gel process described elsewhere [18]. The two precursor solutions, here denoted precursor A and B, were prepared as follows. Precursor A: Titanium (IV) isopropoxide (40 ml), ethanol (50 ml) and acetic acid (3.0 ml) were mixed and stirred for 10 min at room temperature. Precursor B: distilled water (7.0 ml) and ethanol (50 ml) were mixed and the crystallized powders of $Er_{0.01}$-YAG and/or $Er_{0.01}$-YAP (0.5 g) were added under vigorous stirring to make them dispersed adequately in the solution. Afterwards, the precursor B was added to the precursor A drop wise with vigorous stirring. The resultant mixture was further stirred for 20 min. The sol solution was placed in a culture dish for a day to finish the sol-gel transition and filtered. Filter residue was rinsed with water repeatedly, and then dried at 100 °C for 24 h to get a dried gel. The dried gel was ground and a light-yellow powder was obtained. The powder was then heat treated at 400 °C and 700 °C for 2.0 h (ramp 10 °C.min^{-1}) to get a stable TiO_2 photocatalyst coating crystallized $Er_{0.01}$-YAG and/or $Er_{0.01}$-YAP. The ratio of ($Er_{0.01}$-YAG + $Er_{0.01}$-YAP) to TiO_2 in the photocatalyst is about 2.0 %. The pure TiO_2 powder was also prepared using the same procedure without the addition of the upconversion luminescence agents during sol-gel process. The surface areas were determined as 68 and 59 $m^2.g^{-1}$, respectively, for pure TiO_2 and TiO_2 coating crystallized upconversion luminescence agents annealed at 700°C according to BET method.

Catalyst characterization: The X-ray diffraction (XRD) patterns obtained on a D5000X-ray diffractometer (German Bruker) using Cu Kα radiation at a scan rate of 0.02° s^{-1} were used to decide the crystallite size and identity. The average crystallite size was determined according to

the Scherrer equation. The transmission electron micrographs (TEM) were recorded with a JEM-3010 (JEOL Company, Japan) electron microscope and were used for observing the shape of prepared particles and estimating the particle size.

Photoreactor system and experimental procedures: A Pyrex cylindrical photoreactor was used in the experiments, where a 250 W halogen lamp with emission between 400-800 nm and main emission peak at 650 nm was positioned at the center of the cylindrical vessel and surrounded by a circulating water jacket. The UV emission of the lamp is filtered to approximate to sunlight. The intensity of the emitted light of the lamp was obtained by using radiometric calibration standard (Ocean Optics) and is about 140 $W.m^{-2}$. The reactor, which was wrapped with aluminum foil to prevent the loss of light was immersed into a water bath for maintaining a reaction temperature at 25 °C. A magnetic stirrer was used to induce continuous mixing of the reaction solution throughout the experimental period. The photocatalytic degradation of methylene blue (MB) was employed to investigate the photodegradation effect of the TiO_2 catalyst doped with upconversion luminescence agents. The experiments of the photocatalytic degradation of MB in aqueous solution were carried out under the conditions such as 30 $mg.l^{-1}$ MB concentration, 1.0 $g.l^{-1}$ prepared photocatalyst and 125 ml total volume. All photocatalytic experiments were carried out at natural solution pH equal to 6.5. Absorbance measurements were recorded using a UV-Vis spectrophotometer (PerkinElmer Lambda 25 UV-Vis). The wavelength of 665 nm, the maximum absorption wavelength registered experimentally, was used for evaluation of the MB photodegradation. The photocatalytic degradation rate (DR) was calculated by the following formula:

$$DR\ (\%) = (1 - C_t/C_0) \times 100 \qquad (1)$$

Where C_0 is the initial concentration and C_t is the concentration of the MB dye solution at the irradiation time (t).

Total organic carbon (TOC) was determined by using a TOC-Ve Analyzer (Shimadzu) to follow the mineralization of MB.

Outdoor Photocatalytic tests were also carried out under solar light irradiation using the same conditions as under lamp excitation, such as V = 125 ml, 1 $g.l^{-1}$ photocatalyst, 30 $mg.l^{-1}$ MB concentration. The cylindrical photoreactor was directly exposed to sunlight.

Blank tests are performed under the following conditions: (a) MB solution + irradiation, (b) MB solution + photocatalyst (pure TiO_2 or Er-YAG/Er-YAP/TiO_2) in the dark. The results show that the efficiency of the degradation based on the self-photosensitized process is very lower than that using photocatalysis with TiO_2 coating crystallized upconversion luminescence agents. Moreover, it reveals that prepared photocatalysts all behave a little adsorption to MB molecules in aqueous solution.

RESULTS AND DISCUSSION

XRD of $Er_{0.01}$-YAG and $Er_{0.01}$-YAP

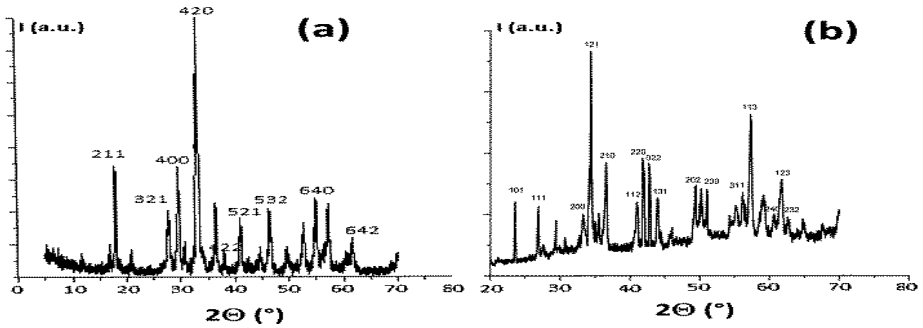

Fig.1. XRD of (a) $Er_{0.01}Y_{2.99}Al_5O_{12}$ and (b) $Er_{0.01}Y_{0.99}AlO_3$ powders.

Fig. 1 shows the XRD patterns of $Er_{0.01}$-YAG (a) and $Er_{0.01}$-YAP (b) powders. It shows that the $Er_{0.01}$-YAG powder heat-treated at 900 °C and the $Er_{0.01}$-YAP powder heated at 1200 °C present crystallized forms. The obtained diffraction peaks of $Er_{0.01}$-YAG are in good agreement with the reference data of $Y_3Al_5O_{12}$ (JCPDS file card 33–40) and the XRD pattern of $Er_{0.01}$-YAP exhibit dominant diffraction peaks due to the orthorhombic phase of $YAlO_3$ (JCPDS File no. 70-1677). The main peaks of both structures are centered at $2\theta = 33.5°$ for $Er_{0.01}$-YAG and $2\theta = 34.5°$ for $Er_{0.01}$-YAP. Both patterns present a well-defined one fold crystal structure and no secondary impurity phase such as $Y_4Al_{12}O_9$ is observed. These findings are similar to those obtained by other researchers [25-26].

XRD and TEM of prepared TiO_2 photocatalyst coating upconversion luminescence agents: Fig. 2 (a, b) shows the XRD patterns of the prepared powders. It can be seen that for pure TiO_2 powder annealed at 400 °C (a), the XRD pattern reveals only anatase phase which is characterized by the main peaks observed at $2\theta = 25, 38, 48, 54, 56, 62.5$ and 68°. The pure anatase phase is still stable even at 700 °C when TiO_2 powder is coating (1.5 % $Er_{0.01}$-YAG + 0.5 %$Er_{0.01}$-YAP) (b) which shows that the upconversion luminescence agents have to increase the thermal stability of this phase (XRD of pure TiO_2 heated at 700 °C, not shown here, reveals both anatase and rutile phases). Moreover, the XRD pattern of TiO_2 coating both $Er_{0.01}$-YAG and $Er_{0.01}$-YAP shows new lines that have been assigned respectively to upconversion luminescence agents YAG and YAP. These lines imply that the particles of upconversion agents and those of TiO_2 have integrated indeed.

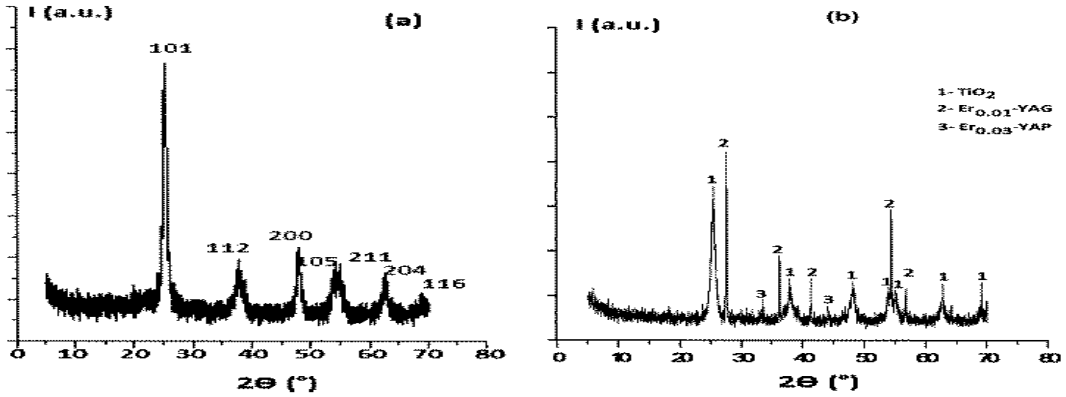

Fig.2. XRD of (a) pure TiO_2 under 400 °C heat-treatment and
(b) (1.5 % $Er_{0.01}$-YAG + 0.5 % $Er_{0.01}$-YAP)/TiO_2 composite under 700 °C heat-treatment.

$$\text{The Scherrer equation: } d = \frac{K\lambda}{\beta \cos\theta} \qquad (2)$$

Was used to calculate the average size of crystallites in each sample, where k = 0.89 is the shape factor of particles, β is the peak width at half maximum (radians).

The sizes of crystallized $Er_{0.01}$-YAG and $Er_{0.01}$-YAP powders are about 20-30 nm. The average size of the prepared TiO_2 is about 50-60 nm when is coating $Er_{0.01}$-YAG or/and $Er_{0.01}$-YAP. Thus, taking into account these sizes, we consider that the layer of TiO_2 particles coating the upconversion agents is suitable for penetrating the visible light and exciting the inner particles of $Er_{0.01}$-YAG and $Er_{0.01}$-YAP, which would result the emission of UV lights.

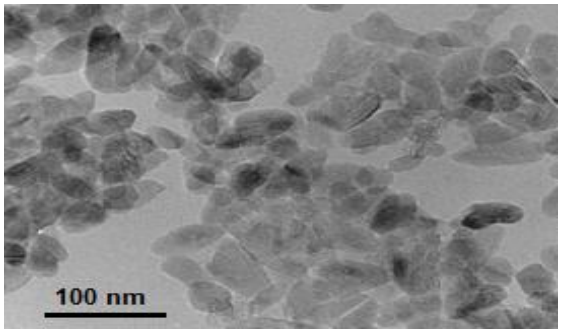

Fig.3. TEM of prepared TiO_2 particles coating $Er_{0.01}$-YAG and $Er_{0.01}$-YAP after 700 °C heat treatment.

Fig.3 shows the TEM image of the prepared TiO_2 powder coating $Er_{0.01}$-YAG and $Er_{0.01}$-YAP. It is found that the prepared TiO_2 powder is composed of grayer particles with approximately uniform size and shape. The average size of these particles estimated from the TEM image is about 50-70 nm. The black parts in central regions of many grayer particles can be found clearly, which can be confirmed as the crystallized upconversion luminescence agents particles covered with TiO_2 folium.

Photocatalytic activity

$Er_{0.01}$-YAG/TiO_2 and $Er_{0.01}$-YAP/TiO_2 photocatalysts : In this part, we show the degradation efficiency of the MB solution (of 30 $mg.l^{-1}$ initial concentration) under the visible light irradiation in the presence of TiO_2 coating one upconversion luminescence agent ($Er_{0.01}$-YAG or $Er_{0.01}$-YAP) in comparison with the prepared pure TiO_2. It can be seen in Fig.4 that the photocatalytic activity of the doped TiO_2 is better than that of the undoped one. The degradation ratio in the presence of TiO_2 powder doped with $Er_{0.01}$-YAG or $Er_{0.01}$-YAP increases with the irradiation time and attains about 96-98% after 5 h, while the degradation ratio in the presence of undoped TiO_2 powder is only 80 % over the same time. These results prove that $Er_{0.01}$–YAG and $Er_{0.01}$-YAP upconversion luminescence agents have improved the photocatalytic activity of TiO_2 photocatalyst.

Since blank tests have shown the weak contribution of self - photosensitized and photolysis processes in the degradation reaction of a MB solution under visible light irradiation, thus, it can be deduced that UV lights resulted from the upconversion process are the major responsible for the improvement of the degradation ratio. These deductions accord well with those found in similar studies of photocatalytic activity via the upconversion luminescence process [18, 27]. However, we think that this improvement could be better if we combine the effect of both upconversion agents $Er_{0.01}$-YAG and $Er_{0.01}$-YAP in coating them together with TiO_2 powders.

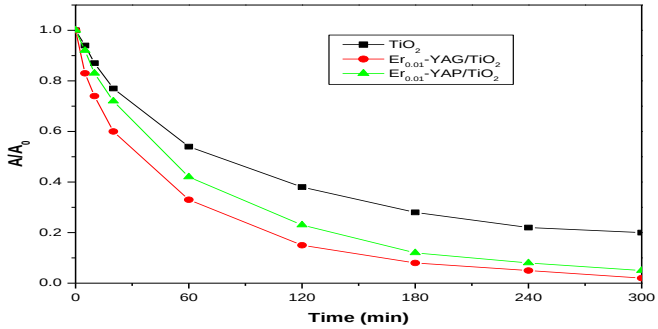

Fig.4. Effect of irradiation time on the photocatalytic degradation of MB solution in the presence of pure TiO_2, $Er_{0.01}$-YAG/TiO_2 and $Er_{0.01}$-YAP/TiO_2 respectively. (C_0 = 30 $mg.l^{-1}$, m_{cat} = 1.0 $g.l^{-1}$, pH = 6.5).

The $Er_{0.01}$-YAG/$Er_{0.01}$-YAP/TiO_2 photocatalyst: The effects of both upconversion luminescence agents $Er_{0.01}$-YAG and $Er_{0.01}$-YAP are combined to get the highest photocatalytic activity of the $Er_{0.01}$-YAG/$Er_{0.01}$-YAP/ TiO_2 composite. The total mass ratio of both agents in the composite is kept equal to 2 %. The following combinations are performed:

(1% $Er_{0.01}$-YAG + 1%$Er_{0.01}$-YAP)/TiO_2.

(1.5% $Er_{0.01}$-YAG + 0.5 %$Er_{0.01}$-YAP)/TiO_2.

(0.5 % $Er_{0.01}$-YAG + 1.5 % $Er_{0.01}$-YAP)/TiO_2.

The photocatalytic tests focus on the degradation of BM solutions under the same conditions as before: [BM] = 30 $mg.l^{-1}$, V = 0.125 l, m (catalyst) = 0.125 g, pH = 6.5 (natural). The photocatalysts are annealed at 700 °C for 2 h.

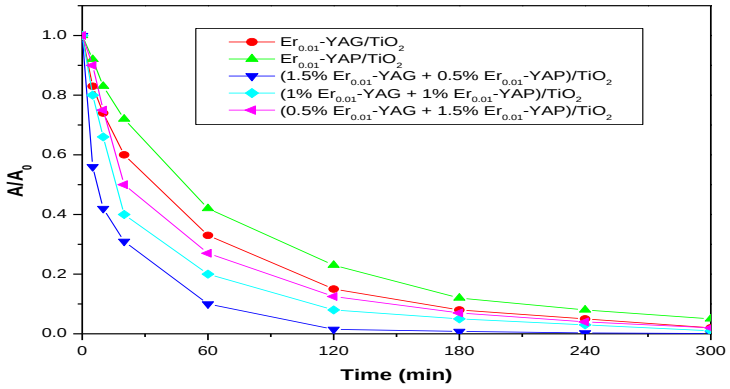

Fig.5. Effect of the combination formula between $Er_{0.01}$-YAG and $Er_{0.01}$-YAP on the photocatalytic activity of $Er_{0.01}$-YAG/$Er_{0.01}$-YAP/TiO_2 composite for the degradation of MB solution.
(C_0 = 30 $mg.l^{-1}$, m_{cat} = 1.0 $g.l^{-1}$, pH = 6.5).

The obtained results are depicted in Fig. 5. In all cases, the degradation ratio of the MB solution in the presence of TiO_2 coating a combination of $Er_{0.01}$-YAG and $Er_{0.01}$-YAP is much more than that obtained in the presence of TiO_2 powder coating only one upconversion luminescence agent. Moreover, the best combination of the upconversion luminescence agents corresponds to 1.5 % $Er_{0.01}$-YAG + 0.5 % $Er_{0.01}$-YAP. The photocatalyst containing 1.5% $Er_{0.01}$-YAG and 0.5% $Er_{0.01}$-YAP has achieved the highest degradation ratio in the short time of irradiation. Indeed, with this composite, almost complete photodegradation of MB solution has been performed after two hours of visible irradiation. This was firstly supported by the deletion of the absorption spectra of MB solution in the UV-Vis range (Fig. 6).

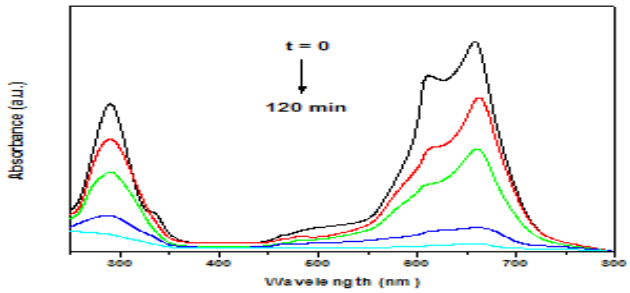

Fig.6. Spectra change that occurs during the degradation of MB aqueous solution irradiated by visible light in the presence of (1.5 % $Er_{0.01}$-YAG + 0.5 % $Er_{0.01}$-YAP)/TiO_2 composite
(C_0 = 30 $mg.l^{-1}$, m_{cat} = 1.0 $g.l^{-1}$, pH = 6.5).

The blue color of MB solution was almost totally deleted after two hours of irradiation. It may mean that the concentration of MB in solution decreased and it was not only solution decolorization but also photodegradation. The total mineralization of methylene blue using (1.5 % $Er_{0.01}$-YAG + 0.5 % $Er_{0.01}$-YAP)/TiO_2 composite was also proved by measuring the initial TOC before irradiation (15.60 ppm) and after two hours of visible irradiation and it was found to be equal to 2.1 ppm. This performance has not been achieved by any of the photocatalysts tested throughout this study such as pure TiO_2, $Er_{0.01}$-YAG/TiO_2 and $Er_{0.01}$-YAP/TiO_2. Indeed, the degradation ratio of MB solution after two hours of visible irradiation is only 62, 77 and 85 % in the presence of pure TiO_2, $Er_{0.01}$-YAP/TiO_2 and $Er_{0.01}$-YAG/TiO_2 respectively. In addition, the modeling of the obtained results by the equation:

$$Ln (C_0/C) = Ln (A_0/A) = k.t \quad (3)$$

shows that the reaction of photocatalytic degradation of MB in the presence of both doped and undoped TiO_2 powders accord with the first order kinetics. The related rate constants (table 1) show that the (1.5 % $Er_{0.01}$-YAG + 0.5 % $Er_{0.01}$-YAP)/TiO_2 composite increases the kinetic reaction more than three times compared to $Er_{0.01}$-YAP/TiO_2 or $Er_{0.01}$-YAG/TiO_2 and more than seven times compared to the prepared pure TiO_2. All these findings allow considering that the combination of both $Er_{0.01}$-YAG and $Er_{0.01}$-YAP leads to an intensification of UV lights from the upconversion process compared to those obtained when only one upconversion luminescence agent is used. The photodegradation efficiency is, therefore, highly improved.

Table 1: Rate constants of the degradation reaction of the MB solution in the presence of various photocatalysts under visible irradiation (C_0 = 30 mg.l^{-1}, m_{cat} = 1.0 g.l^{-1}, pH = 6.5).

Photocatalyst	k 10^3 (min^{-1})	R^2
TiO_2	3	0.96
$Er_{0.01}$-YAP/TiO_2	5	0.99
$Er_{0.01}$-YAG/TiO_2	7	0.97
(0.5% $Er_{0.01}$-YAG +1.5% $Er_{0.01}$-YAP)/TiO_2	8	0.95
(1% $Er_{0.01}$-YAG + 1% $Er_{0.01}$-YAP)/TiO_2	9	0.93
(1.5%$Er_{0.01}$-YAG + 0.5% $Er_{0.01}$-YAP)/TiO_2	21	0.99

In order to more investigate the kinetics of the photocatalytic degradation of MB in the presence of (1.5 % $Er_{0.01}$-YAG + 0.5 % $Er_{0.01}$-YAP)/TiO_2 composite irradiated by visible light, the rate constant (k) of the degradation reaction has been studied in relation to the initial concentration of MB solution (C_0). Table 2 reports the values of k resulting from the plot of Ln (C_0/C) versus time for the photocatalytic degradation of MB, which decreases as the initial reactant concentration increases. This can be ascribed to the decrease in the number of active sites on the catalyst surface due to the covering of the surface with MB molecules, which is directly proportional to the initial concentration of MB.

Table 2: kinetic rate constant of photocatalytic degradation of MB in the presence of (1.5 % $Er_{0.01}$-YAG + 0.5 % $Er_{0.01}$–YAP)/TiO_2 composite under visible light with different initial concentration (pH = 6.5).

$C_0 = [MB]_0$ (mg.l^{-1})	k (min^{-1})
5	0.037
10	0.030
20	0.026
30	0.021

The experimental data has been rationalized in terms of the modified form of Langmuir-Hinshelwood (L-H) kinetic model to describe the solid-liquid reaction successfully. The effect of the initial concentration of MB on the initial degradation rate (r) is given by the following equations:

$$r = K_{MB} .k_c [C]. (1 + K_{MB}. [C_0])^{-1} = k [C] \quad (4)$$

$$1/k = 1/K_{MB}.k_c + [C_0]/k_c \quad (5)$$

Where, K_{MB} and k_c are the L-H adsorption equilibrium constant and the rate constant of surface reaction, respectively. At concentrations up to 30 $mg.l^{-1}$, the applicability of the L-H equation for the photocatalytic degradation of MB has been confirmed by the linear plot obtained by plotting the reciprocal of the rate constant (1/k) against the initial concentration ($[C]_0$) (not shown here). The values of K_{MB} and k_c are found to be 0.336 ($mg^{-1}.l$) and 0.149 $mg.l^{-1}.min^{-1}$, respectively.

Determination of the Quantum Yield: The quantum yield (Φ) is a useful parameter in indicating the efficiency of a photodegradation reaction, and is defined as the number of molecules being decomposed per photon absorbed. It can be calculated from the observed first-order degradation rate constant as follows:

$$\Phi = k / 2.303\ \varepsilon_\lambda\ I_{0,\lambda}\ l \quad (6)$$

Where k (s^{-1}) is the pseudo-first-order rate constant, $I_{0,\lambda}$ (Einstein $l^{-1}s^{-1}$) is the incident light intensity at wavelength λ which has been calculated on the bases of the ferrioxalate actinometry measurements, ε_λ ($cm^{-1}M^{-1}$) is the molar absorptivity at wavelength λ, and l is the cell path length (cm).

The quantum yield values for the photodegradation of MB by direct photolysis and in the presence of (1.5 % $Er_{0.01}$-YAG + 0.5 % $Er_{0.01}$-YAP)/TiO_2 composite irradiated by a visible lamp at λ_{max} = 650 nm are 0.007 and 0.11, respectively. These results indicate that the photocatalysis quantum yield in the presence of (1.5 % $Er_{0.01}$-YAG + 0.5 % $Er_{0.01}$-YAP)/TiO_2 is higher than that of the direct photolysis, suggesting that the photodecay of MB is dominated by the photocatalysis.

It has to be mentioned that, since r = f (C) follows a Langmuir-Hinshelwood mechanism, with a linear increase of r at low concentrations, this catalytic quantum yield could be consequently higher for higher concentrations. It is high enough to ensure a reasonable degradation rate for diluted colored water solutions.

Photocatalytic activity of $Er_{0.01}$-YAG/$Er_{0.01}$-YAP/TiO_2 under sunlight: After being selected as the most effective photocatalyst resulting from the combination of both $Er_{0.01}$-YAG and $Er_{0.01}$-YAP, the (1.5 % $Er_{0.01}$-YAG + 0.5 % $Er_{0.01}$-YAP)/TiO_2 composite is evaluated under sunlight excitation in comparison with visible light excitation from the halogen lamp. The outdoor experiments (Gabes city, Tunisia) are carried out from a.m. 09:00 to p.m. 14:00 of 10-15 June 2012, where the corresponding temperature varied from 30 to 35 °C, respectively. The obtained results (Fig.7) show that the (1.5% $Er_{0.01}$-YAG + 0.5% $Er_{0.01}$-YAP)/TiO_2 composite is very active under sunlight. Indeed, the irradiation time needed to attain a degradation ratio of about 100 % is reduced to half (60 min) compared to that shown with visible irradiation from the 250 W halogen lamp (120 min) in the presence of the same photocatalyst. Furthermore, the rate constant (0.071 min^{-1}) is more than three times higher than that found if visible irradiation is used (0.021 min^{-1}). Considering the treatment cycle cost, shortening time for the MB treatment is a necessary goal that is achieved with the use of solar light in the presence of the (1.5% $Er_{0.01}$-YAG + 0.5% $Er_{0.01}$-YAP)/TiO_2 composite. This performance, which is comparable to those reached when using UV lights directly from the artificial lamp for treating dyes by TiO_2 photocatalyst [26], may be explained by the contribution of about 4-5% of sun lights which are in the form of UV radiations, more energetic than visible lights for the excitation of electrons from the valence to the conduction band of TiO_2. Besides, the solar lights contain continuous pump wavelengths that make the upconversion process take place more easily in $Er_{0.01}$-YAG and $Er_{0.01}$ –YAP crystals compared to the visible lights from the 250 W power lamp. It is also worthy to notice the improvement of the degradation ratio in the presence of pure TiO_2 under sunlight containing UV radiations, but this improvement is still lower than that attained with the new $Er_{0.01}$-YAG/$Er_{0.01}$-YAP/TiO_2 photocatalyst.

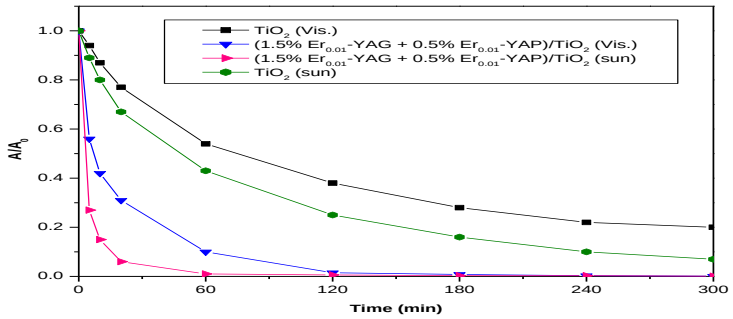

Fig.7. Comparison of the photocatalytic activity of (1.5 % $Er_{0.01}$-YAG + 0.5 % $Er_{0.01}$–YAP)/TiO_2 composite and pure TiO_2 under solar and visible light irradiation for the degradation of MB solution. (C_0 = 30 mg.l^{-1}, m_{cat} = 1.0 g.l^{-1}, pH = 6.5).

Photocatalytic activity of $Er_{0.01}$-YAG/$Er_{0.01}$-YAP/TiO_2 for the degradation of some other dyes under sunlight : The photocatalytic activity of (1.5% $Er_{0.01}$-YAG +0.5% $Er_{0.01}$-YAP)/TiO_2 composite under solar light irradiation is also evaluated with other organic dyes having different molecular structures and chemical compositions such as methyl violet (MV), Congo red (CR) and methyl orange (MO). The manipulative experiments are performed in the same conditions as before (with MB) such as 1 g.l^{-1} photocatalyst, 30 mg.l^{-1} dye concentration and natural pH value. The degradation ratio of each dye is measured after 60 min of solar light irradiation using UV-vis spectroscopy at maximum absorption (MV: 590 nm; CR: 541 nm; MO: 465 nm). Fig.8 shows a high degradation ratio for cationic dyes (MB and MV) and lower ratios for anionic ones (CR and MO). This is obviously explained by the electrostatic attraction or repulsion that has occurred between different organic molecules (cationic or anionic) and TiO_2 surface negatively charged at the natural pH value (pH = 6.5). Thus, the degradation ratio of anionic dyes should be higher in the more acidic medium. This was highly supported by experimental results obtained when varying pH conditions in the photocatalytic tests (Table 3). The pH effect can be explained by the zero point of charge of TiO_2 surface, usually around 6. The surface of the photocatalyst is positively charged in acidic solutions and negatively charged in neutral and alkaline solutions. As a result, it is not surprising to observe an increase in the adsorption of cationic dye molecules on the surface of photocatalyst in alkaline solutions, leading to an increase in the degradation efficiency of dye. But at low pH, the adsorption of cationic dyes on the positively charged surface of the photocatalyst decreases due to repulsive forces, leading to a decrease in the degradation efficiency. For the anionic dyes, they behave reversely with pH.

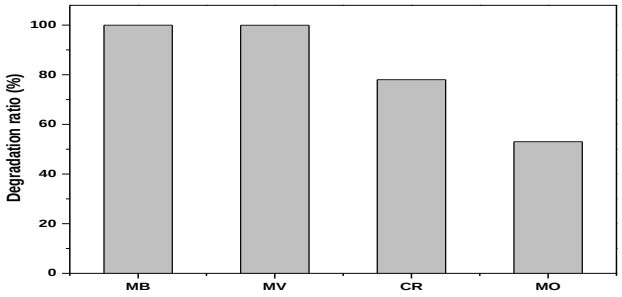

Fig.8. Degradation ratios of various organic dyes in the presence of (1.5 % $Er_{0.01}$-YAG + 0.5 % $Er_{0.01}$–YAP)/TiO_2 composite under solar light irradiation (C_0 = 30 mg.l^{-1}, m_{cat} = 1.0 g.l^{-1}, pH = 6.5).

With reference to experimental results, the (1.5% $Er_{0.01}$-YAG + 0.5% $Er_{0.01}$-YAP)/TiO_2 composite shows promise in solar energy applications when the pH conditions are optimized.

Table 3: Degradation ratios (DR) of MB (cationic) and MO (anionic) dyes in the presence of (1.5 % $Er_{0.01}$-YAG + 0.5 % $Er_{0.01}$–YAP)/TiO_2 composite under solar light irradiation at three different pH solutions.

pH	DR (%) of MB	DR (%) of MO
3.5	58	92
6.5	98	53
9	96	51

Mechanism discussion: Er^{3+}: YAG and Er^{3+}: YAP are known as efficient upconversion agents that enable the visible light to transform into the UV light. For the Er^{3+}: YAP, the emission bands around 318.7 and 320.1 nm were observed under the pumping of 486.5 and 542.4 (or 548.8) nm visible light [24, 27], respectively. In addition, the 326-312 nm and 354-359 nm upconversion luminescence by 652.2 (or 657.8) nm pumping was also detected [28]. Many other emission bands of wavelengths inferior to that of excitation source are also observed [21]. When Er^{3+}:YAG as the upconversion luminescence agent is pumped by a 488 nm Ar^+ laser, the upconversion signals at 271, 317 and 381 nm are observed. Otherwise, the upconversion signal at 320 nm is also found by a 647 nm laser excitation [19, 20]. The solar light (and its visible section) which contains continuous pump wavelengths was used as an excitation source, thus the upconversion process may easily take place in Er^{3+}: YAG and Er^{3+}: YAP crystals. If both Er^{3+}:YAG and Er^{3+}:YAP are excited at the same time with continuous visible light, the upconversion signal should contain all their emission bands leading to an intensification of the emitted light from the upconversion process. According to the energy level data given in references [16, 21, 22], the upconversion process can be achieved through the chains of ground state absorption (GSA) and excited state absorption (ESA). As illustrated in fig. 9, the crystallized Er^{3+}:YAG and Er^{3+}:YAP as upconversion luminescence agents coated by the TiO_2 folium, under continuous excitation of visible light, can emit the UV light, which can effectively be absorbed by TiO_2 parts to generate the electron-hole pairs. The holes not only directly decompose the MB adsorbed on the surface of TiO_2 particles, but also oxidize water molecules to form ·OH radicals with high activity and indirectly degrade the MB in the aqueous solution.

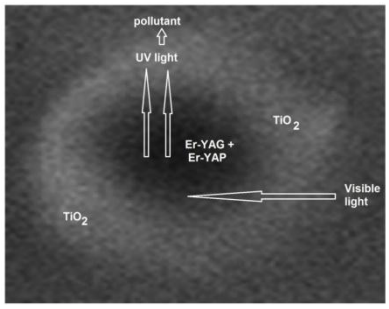

Fig.9. Degradation processes of organic dyes catalyzed by $Er_{0.01}$-YAG/$Er_{0.01}$-YAP/TiO_2 composite under solar light irradiation.

APPLICATION

The Er-YAG/Er-YAP/TiO_2 composite shows high efficiency as a photocatalyst for the degradation reaction of some dye aqueous solutions under visible and solar lights. It is able to convert visible lights into more energetic UV lights. Thus, using the upconversion mechanism, the $Er_{0.01}$-YAG/$Er_{0.01}$-YAP/TiO_2 could be used as an efficient photocatalyst for treating dyes aqueous solutions under sunlight irradiation.

CONCLUSION

A new photocatalyst with high catalytic activity under visible and solar irradiation is prepared. It is based on TiO_2 coating a combination of two upconversion luminescence agents: $Er_{0.01}$-YAG and $Er_{0.01}$-YAP. The $Er_{0.01}$-YAG/$Er_{0.01}$-YAP/TiO_2 composite is prepared by the sol - gel method. This composite is found to be more photoactive than pure TiO_2 and both $Er_{0.01}$-YAG/TiO_2 and $Er_{0.01}$-YAP/TiO_2. The (1.5 % $Er_{0.01}$-YAG + 0.5 % $Er_{0.01}$–YAP)/TiO_2 combination is found to have the highest photocatalytic activity for the degradation of MB in aqueous solution under visible and solar light irradiation. Shortening time for the MB treatment is a necessary goal that is achieved with the use of solar light in the presence of the (1.5% $Er_{0.01}$-YAG + 0.5% $Er_{0.01}$-YAP)/TiO_2 composite. The irradiation time needed to achieve a degradation ratio of about 100 % is reduced to half compared to that shown with visible irradiation from the 250 W halogen lamp. Some other dyes exhibit high degradation ratios in the presence of this composite. Therefore, the $Er_{0.01}$-YAG/$Er_{0.01}$-YAP/TiO_2 composite combining the effect of two upconversion luminescence agents may be envisaged as a novel photocatalyst for treating aqueous dye solutions using solar energy.

REFERENCES

[1] M.R. Hoffmann, S.T. Martin, W. Choi, D.W. Bahnemannt, *Chem. Rev*. **1995**, 95, 69-96.
[2] A. Houas, H. Lachheb, M. Ksibi, E. Elaloui, C. Guillard, J.M. Hermann, *Appl. Catal. B: Environ*. **2001**, 31, 145-157.
[3] X.B. Chen, S.S Mao, *Chem. Rev*. **2008**, 107, 2891-2959.
[4] J.Q. Zhang, Z.C. Xu, M.J. Feng, C. Li, *Angew. Chem. Int. Ed* **2008**, 47, 1766-1769.
[5] G. Liu, Y.N. Zhao, C.H. Sun F. , Li, G.Q. Lu, H.M. Cheng, *Angew. Chem. Int. Ed* **2008**, 47, 4516-4520.
[6] T. Ohno, M. Akiyoshi, T. Umebayashi, K. Asai, T. Mitsui, M. Matsumura, *Appl. Catal. A: General* **2004**, 265, 115-121.
[7] U. Diebold, *Surf. Sci. Rep.* **2003**, 229, 48-53.
[8] P.V. Kamat, *Chem. Rev.* **1993**, 93, 267-300.
[9] R. Asahi, T. Morikawa, T. Ohwaki, K. Aoki, Y. Taga, *Science* **2001**, 293, 269-271.
[10] K. Kobayakawa, Y. Murakami, Y. Sato, *J. Photochem Photobiol A: Chem* **2005**, 170, 177-179.
[11] M.F. Joubert, *Opt. Mater*. **1999**, 11, 181-203.
[12] R. Francini, S. Pietrantoni, M. Zambelli, A. Speghini, M. Bettinelli, *J. Alloy. Compd*. **2004**, 380, 34-38.
[13] C. Strümpel, M. MCCann, G. Beaucarne, V. Arkhipov, A. Slaoui, V. švrček, C. Del Cañizo, I. Tobias, *Sol. Energy Mater. Sol. C.* **2007**, 91, 238-249.
[14] S. Georgescu, O. Toma, C. Florea, C. Naud, *J. Lumin*. **2003**, 101, 87-99.
[15] N.] Jaba, A. Kanoun, H. Mejri, A. Selmi, S. Alaya, H. Maaref, *J. Phys: Condens. Matter*. **2000**, 12, 4523-4534.
[16] N. Zu, H. Yang, Z. Dai, *Physica B.* **2008**, 403, 174-177.
[17] J. Wang, F.Y. Wen, Z.H. Zhang, X.D. Zhang, Z.J. Pan, P. Zhang, P.L. Kang, J. Tong, L. Wang, L. Xu, *J. photochem. Photobiol. A: Chem*. **2006**, 180, 189-195.
[18] J. Wang, R. Li, Z. Zhang, W. Sun, R. Xu, Y. Xie, Z. Xing, X. Zhang, *Appl. Catal. A: General*. **2008**, 334, 227-233.
[19] J. Wang, J. Li, Y. Xie, C. Li, G. Han, L. Zhang, R. Xu, X. Zhang, *J. Environ. Manag.* **2010**, 91, 677-684.
[20] H. Xu, Z. Jiang, *Chem. Phy.* **2003**, 287, 155-159.

[21] H. Yang, Z. Dai, Z. Sun, *J. Lumin.* **2007,** 124, 207-212.
[22] H.L. Xu, S. KrÖll, *J. Lumin.* **2005**, 111, 191-198.
[23] E. De la Rosa, L.A. Diaz-Torres, P. Salas, A. Arredondo, J.A. Montoya, C. Angeles, R.A. Rodriguez, *Opt. Mater*. **2005**, 27, 1793-1799.
[24] P.A. Tanner, P.T. Law, K.L. Wong, L.S. Fu, *J. Mater. Sci.* **2003**, 38, 4857-4861.
[25] H.M.H. Fadlalla, C.C. Tang, A. Elsanousi, X.X. Ding, S.R. Qi, *J. Lumin.* **2009**, 129, 401–405.
[26] H.B. Premkumar, DV Sunitha, H Nagabhushana, S.C. Sharma, B.M. Nagabhushana, C. Shivakumara, J.L. Rao, R.P.S. Chakradhar., *J. Lumin.* **2013**, 135, 105–112.
[27] J. Wang, Y. Xie, Z. Zhang, J. Li, X. Chen, L. Zhang, R. Xu, X. Zhang, *Sol. Energy Mat. Sol. C.* **2009**, 93, 355–361.
[28] J. Li, W. Ma, C. Chen, J. Zhao, H. Zhu, X.Gao, *J. Mol. Catal. A: Chem.* **2007**, 261, 131-138.